

# Complete Toy Models of Holographic Duality

Tamara Kohler<sup>1</sup> and Toby Cubitt<sup>1</sup>

<sup>1</sup>Department of Computer Science, University College London, UK

## Abstract

Tensor networks have previously been used to construct holographic quantum error correcting codes (HQECC), which are toy models of the AdS/CFT correspondence. HQECC have been able to exhibit many of the interesting features of the duality, such as complementary recovery and redundant encoding. However, in previous HQECC the boundary Hamiltonian which results from mapping a local bulk Hamiltonian to the boundary is a non-local Hamiltonian, with global terms that act over the entire boundary. In this work, we combine HQECC with recently developed Hamiltonian simulation theory to construct a bulk-boundary mapping in which local bulk Hamiltonians map to local boundary Hamiltonians. This allows us to construct a toy model of a complete holographic duality between *models*, not just states and observables. This mapping of local Hamiltonians extends the toy models to encompass the relationship between bulk and boundary energy scales, and in particular the mapping between bulk and boundary time dynamics. We discuss what insight this gives into toy models of black hole formation.

# Contents

<b>1</b>	<b>Introduction</b>	<b>4</b>
<b>2</b>	<b>Main results</b>	<b>5</b>
2.1	Proof overview . . . . .	6
<b>3</b>	<b>Preliminaries</b>	<b>8</b>
3.1	Perfect tensors and pseudo-perfect tensors . . . . .	8
3.1.1	(Pseudo-)perfect tensors and absolutely maximally entangled states . . . . .	8
3.1.2	(Pseudo-)perfect tensors and quantum error correcting codes . . . . .	9
3.1.3	Existence of (pseudo-)perfect tensors . . . . .	11
3.2	Qudit stabilizer codes and states . . . . .	12
3.2.1	Generalised Pauli group . . . . .	12
3.2.2	Qudit stabilizer codes . . . . .	12
3.2.3	Qudit stabilizer codes and (pseudo-)perfect tensors . .	12
3.3	Existence of (pseudo-)perfect stabilizer tensors . . . . .	17
3.3.1	Classical coding theory . . . . .	17
3.3.2	Constructing AME stabilizer states . . . . .	18
3.4	Hyperbolic Coxeter groups . . . . .	18
3.4.1	Coxeter systems . . . . .	18
3.4.2	Combinatorics of Coxeter groups . . . . .	20
3.4.3	Growth rates of Coxeter groups . . . . .	21
3.4.4	Coxeter groups in $\mathbb{H}^3$ . . . . .	21
3.5	Hamiltonian simulation . . . . .	23
3.5.1	Hamiltonian encodings . . . . .	23
3.5.2	Hamiltonian simulation . . . . .	24
3.5.3	Perturbation gadgets . . . . .	24
3.5.4	Perturbative simulations . . . . .	30
<b>4</b>	<b>Holographic quantum error correcting codes and complete bulk-boundary dualities</b>	<b>31</b>
4.1	Notation . . . . .	31
4.2	General construction . . . . .	32
4.2.1	Holographic quantum error correcting codes . . . . .	32
4.2.2	Surface of the HQECC . . . . .	34
4.2.3	The metric on the boundary surface of the HQECC .	41
4.2.4	Operators on the boundary surface of the HQECC .	42
4.2.5	A complete holographic duality . . . . .	44
4.3	HQECC constructed from pentagonal prisms . . . . .	50
4.3.1	Perfect tensor . . . . .	51
4.4	HQECC based on the order-4 dodecahedral honeycomb . .	52

4.4.1	Pseudo-perfect tensor	54
<b>5</b>	<b>Discussion</b>	<b>55</b>
5.1	Main result	55
5.2	Black hole formation in HQECC	55
5.3	Other geometries	57
<b>6</b>	<b>Conclusions</b>	<b>58</b>

# 1 Introduction

The AdS/CFT correspondence is a conjectured duality between quantum gravity in  $(d+1)$  dimensional asymptotically AdS space, and a conformal field theory defined on its boundary [28]. It has provided insight into theories of quantum gravity, and has also been used as a tool for studying strongly-interacting quantum field theories. Recently it has been shown that important insight into the emergence of bulk locality in AdS/CFT can be gained through the theory of quantum error correcting codes [3]. This idea has been used to construct holographic quantum error correcting codes (HQECC) [31, 39, 38, 43, 21], which realise many of the interesting structural features of AdS/CFT.

Holographic quantum codes give a map from bulk to boundary Hilbert space, hence also from observables in the bulk to corresponding boundary observables. But the AdS/CFT correspondence is also a mapping between *models*, not just between states and observables; it relates quantum theories of gravity in the bulk to conformal field theories in one dimension lower on the boundary. For holographic code models, this means realising a mapping between local Hamiltonians in the bulk and local Hamiltonians on the boundary.

Since holographic quantum codes give a mapping from any bulk operator to the boundary, one can certainly map any local bulk Hamiltonian to the boundary. But this gives a completely non-local boundary Hamiltonian, with global interactions that act on the whole boundary Hilbert space at once. Local *observables* deep in the bulk are expected to map under AdS/CFT duality to non-local boundary observables, so this is fine – indeed, expected – for observables. But a global Hamiltonian acting on the entire boundary Hilbert space has lost all relation to the boundary geometry; there is no meaningful sense in which it acts in one dimension lower. Indeed, for toy spin models, any Hamiltonian whatsoever can be realised using a global operator. For the correspondence between bulk and boundary models to be meaningful, the local Hamiltonian describing the bulk physics needs to map to a *local* Hamiltonian on the boundary. For this reason, [31] study the mapping of observables and states in their construction, and do not apply it local Hamiltonians.

By standing on the shoulders of the holographic quantum code results, in particular the HaPPY code [31], and combining stabilizer code techniques with the recent mathematical theory of Hamiltonian simulation [9], we build on these previous results to construct a complete holographic duality between 3D hyperbolic space and its 2D boundary. This allows us to extend the toy models of holographic duality in previous HQECC to encompass Hamiltonians, and in doing so enables us to say something about how energy scales and dynamics in the bulk are reflected in the boundary.

The remainder of the paper is set out as follows. In Section 2 we present

our main result, and give an overview of the proof. In Section 3 we introduce the background required to understand the construction, and prove a number of lemmas which are used in the main result. In Section 4.2 we set out the general procedure for constructing a HQECC in  $\mathbb{H}^3$ , and prove our main result: that there exists a complete holographic duality between  $\mathbb{H}^3$  and its 2D boundary. The proof does not rely on the properties of any particular HQECC, and holds provided that there exists a HQECC in  $\mathbb{H}^3$ . In Section 4.3 and Section 4.4 we provide two examples of HQECC in  $\mathbb{H}^3$ . Finally in Section 5 we discuss the implications of our results, including a toy model of black hole formation within these HQECC.

## 2 Main results

In this paper we construct a complete duality between  $\mathbb{H}^3$  and its 2D boundary. Our main results are encapsulated in the following theorem:

**Theorem 2.1.** *Let  $\mathbb{H}^3$  denote 3D hyperbolic space, and let  $B_r(x) \subset \mathbb{H}^3$  denote a ball of radius  $r$  centred at  $x$ . Consider any arrangement of  $n$  qudits in  $\mathbb{H}^3$  such that, for some fixed  $r$ , at most  $k$  qudits and at least one qudit are contained within any  $B_r(x)$ . Let  $L$  denote the minimum radius ball  $B_L(0)$  containing all the qudits (which wlog we can take to be centred at the origin). Let  $H_{\text{bulk}} = \sum_Z h_Z$  be any local Hamiltonian on these qudits, where each  $h_Z$  acts only on qudits contained within some  $B_r(x)$ .*

*Then we can construct a Hamiltonian  $H_{\text{boundary}}$  on a 2D boundary manifold  $\mathcal{M} \in \mathbb{H}^3$  with the following properties:*

1.  *$\mathcal{M}$  surrounds all the qudits, has diameter  $O\left(\max(1, \frac{\ln(k)}{r})L + \log \log n\right)$ , and is homeomorphic to the Euclidean 2-sphere.*
2. *The Hilbert space of the boundary consists of a triangulation of  $\mathcal{M}$  by triangles of  $O(1)$  area, with a qubit at the centre of each triangle, and a total of  $O(n(\log n)^2)$  triangles/qubits.*
3. *Any local observable/measurement  $M$  in the bulk has a set of corresponding observables/measurements  $\{M'\}$  on the boundary with the same outcome. A local bulk operator  $M$  can be reconstructed on a boundary region  $A$  if  $M$  acts within the greedy entanglement wedge of  $A$ , denoted  $\mathcal{E}[A]$ .<sup>1</sup>*
4.  *$H_{\text{boundary}}$  consists of 2-local, nearest-neighbour interactions between the boundary qubits. Furthermore,  $H_{\text{boundary}}$  can be chosen to have full*

---

<sup>1</sup>The entanglement wedge,  $\mathcal{E}_A$  is a bulk region constructed from the minimal area surface used in the Ryu-Takayanagi formula. It has been suggested that on a given boundary region,  $A$ , it should be possible to reconstruct all operators which lie in  $\mathcal{E}_A$  [27]. The greedy entanglement wedge is a discretised version defined in [31, Definition 8]

local  $SU(2)$  symmetry; i.e. the local interactions can be chosen to all be Heisenberg interactions:  $H_{\text{boundary}} = \sum_{\langle i,j \rangle} \alpha_{ij} (X_i X_j + Y_i Y_j + Z_i Z_j)$ .

5.  $H_{\text{boundary}}$  is a  $(\Delta_L, \epsilon, \eta)$ -simulation of  $H_{\text{bulk}}$  in the rigorous sense of [9, Definition 23], with  $\epsilon, \eta = 1/\text{poly}(\Delta_L)$ ,  $\Delta_L = \Omega((\max_Z \|h_Z\|)^{\text{poly}(n \log(n))})$  and  $|\alpha_{ij}| \leq \Delta_L$ .

This result allows us to extend toy models of holographic duality such as [31] to include a mapping between Hamiltonians. In doing so we show that the expected relationship between bulk and boundary energy scales can be realised by local boundary models. In particular, in our construction toy models of static black holes (as proposed in [31]) correspond to high-energy states of the local boundary model, as would be expected in AdS/CFT.

Moreover, in our toy model we can say something about how dynamics in the bulk correspond to dynamics on the boundary. Even without writing down a specific bulk Hamiltonian we are able to demonstrate that the formation of a (toy model) static black hole in the bulk corresponds to the boundary unitarily evolving to a state outside of the code space of the HQECC, as expected in AdS/CFT (see Section 5.2 for details).

## 2.1 Proof overview

To construct the bulk/boundary map between Hilbert spaces, observables and local Hamiltonians described by Theorem 4.9, we combine new tensor network constructions of HQECC inspired by [31], with perturbation gadget techniques originally developed in Hamiltonian complexity theory. We then use the recently developed theoretical framework of analogue Hamiltonian simulation [9] to show that this gives a complete duality between the bulk and boundary physics.

[31] constructs a HQECC by building a tensor network composed out of perfect tensors, arranged in a tessellation of hyperbolic 2-space by pentagons. This gives a map from 2D bulk to 1D boundary. However, the Hamiltonian simulation constructions of [9] only work in 2D or higher, which means we require at least a 3D bulk and 2D boundary. We must therefore generalise the holographic tensor network codes to 3D as a first step. When working in  $\mathbb{H}^2$  it is possible to use the Poincare disc model to visualise the tessellations and determine their properties. However, in  $\mathbb{H}^3$  this is more difficult, and generalising the HQECC to 3D and higher requires a more systematic approach.

We use hyperbolic Coxeter groups to analyse honeycombs (higher-dimensional tessellations) of  $\mathbb{H}^3$ . (The techniques also generalise beyond 3D.) A Coxeter system is a pair  $(W, S)$ , where  $W$  is a group, generated by a set  $S \subset W$  of involutions, subject only to relations of the form  $(s_i s_j)^{m_{ij}} = 1$  where  $m_{ii} = 1$ ,  $m_{ij} \in (\mathbb{N} \setminus 1) \cup \{\infty\}$  for  $i \neq j$ . Coxeter groups admit a geometric representation as groups generated by reflections. Associated to

every hyperbolic Coxeter system is a Coxeter polytope  $P \subseteq \mathbb{H}^d$ , where  $P$  tessellates  $\mathbb{H}^d$ . All of the properties of the tessellation can be determined directly from the Coxeter system  $(W, S)$  using combinatorics of Coxeter groups. For example, we use the Coxeter relations to prove that the boundary of the HQECC is homeomorphic to the Euclidean 2-sphere.

Generalising the method in [31], we construct tensor networks by taking a Coxeter system  $(W, S)$  with Coxeter polytope  $P \subseteq \mathbb{H}^3$ , and placing perfect tensors in each polyhedral cell of (a finite portion of) the tessellation of  $\mathbb{H}^3$  by  $P$ . Each perfect tensor in the interior of the tessellation has one free index, corresponding to a bulk qudit; the other indices are contracted with neighbouring tensors. Tensors at the outer edge can be shown, again using the Coxeter relations, to have between  $\lceil \frac{t}{2} \rceil$  and  $t - 2$  additional free indices (where the perfect tensor has a total of  $t$  indices), which correspond to qudits on the boundary. We can show that if the tessellation of  $\mathbb{H}^3$  associated to a Coxeter system  $(W, S)$  has the properties required for a HQECC, then the associated Coxeter polytope  $P$  has at least 7 faces, which means we require perfect tensors with at least 8 indices. There are no qubit perfect tensors with  $\geq 6$  indices [14, 33, 25], so we must use qudit perfect tensors.

In order to later generate a local boundary model using perturbation gadgets, we need the tensor network to preserve the Pauli rank of operators. As we are working with qudits rather than qubits, we mean generalised Pauli operators on qudits, rather than qubit Paulis, and we choose prime-dimensional qudits. We use perfect tensors which describe qudit stabilizer absolutely maximally entangled states (AMES), constructed via the method in [22] from classical Reed-Solomon codes. Using properties of stabilizer groups, we show that tensor networks composed of these qudit stabilizer perfect tensors preserve the generalised Pauli rank of operators.

This Coxeter polytope qudit perfect tensor network gives a HQECC in  $\mathbb{H}^3$ . The non-local boundary Hamiltonian is given by  $H'_{\text{boundary}} = H' \Pi_C + \Delta_S (\mathbb{I} - \Pi_C)$ , where  $\Pi_C = VV^\dagger$  is the projector onto the code-subspace of the HQECC,  $V$  is the encoding isometry of the HQECC and  $H'$  satisfies  $VH_{\text{bulk}}V^\dagger = H' \Pi_C = H' VV^\dagger$ .<sup>2</sup> Comparing with the classification of Hamiltonian simulations in [9] it is clear that this mapping is an example of a simulation. (In fact, a perfect simulation in the terminology of [9].)

In order to construct a local boundary Hamiltonian we first determine the distribution of Pauli weights of the terms in  $H'_{\text{boundary}}$  from the properties of the Coxeter system. We then use perturbation gadgets to reduce the boundary Hamiltonian to a 2-local planar Hamiltonian. The techniques we use follow the methods from [30], however the perturbation gadgets derived in [30] can't be used in our construction as the generalised Pauli operators aren't Hermitian. We therefore generalise those to qudit perturbation gadgets which act on operators of the form  $P_A + P_A^\dagger$ , where  $P_A \in \mathcal{G}_{n,p}$ . These gadgets

---

<sup>2</sup> $H'_{\text{boundary}}$  is not unique, as expected in AdS/CFT

meet the requirements in [9, 6] to be perturbative simulations. Finally we use simulation techniques from [9] to simulate the planar 2-local qudit Hamiltonian with a qubit Hamiltonian on a triangular lattice with full local  $SU(2)$  symmetry.

See Section 4.2.5 for the full proof.

## 3 Preliminaries

### 3.1 Perfect tensors and pseudo-perfect tensors

Perfect tensors were first introduced in [31], where they were used in the construction of HQECC from a 2D bulk to a 1D boundary.

**Definition 1** (Perfect tensors, definition 2 from [31]). *A  $2m$ -index tensor  $T_{a_1 a_2 \dots a_{2m}}$  is a perfect tensor if, for any bipartition of its indices into a set  $A$  and a complementary set  $A^c$  with  $|A| \leq |A^c|$ ,  $T$  is proportional to an isometric tensor from  $A$  to  $A^c$ .*

This definition is equivalent to requiring that the tensor is a unitary from any set of  $m$  legs to the complementary set.

For one of the holographic error correcting code constructions in this work we will introduce a generalisation of perfect tensors, which we refer to as pseudo-perfect tensors.

**Definition 2** (Pseudo-perfect tensors). *A  $2m + 1$ -index tensor  $T_{a_1 a_2 \dots a_{2m+1}}$  is a pseudo-perfect tensor if, for any bipartition of its indices into a set  $A$  and a complementary set  $A^c$  with  $|A| < |A^c|$ ,  $T$  is proportional to an isometric tensor from  $A$  to  $A^c$ .*

#### 3.1.1 (Pseudo-)perfect tensors and absolutely maximally entangled states

Perfect and pseudo-perfect tensors are closely related to the concept of absolutely maximally entangled (AME) states, where AME states are states which are maximally entangled across all bipartitions. More formally:

**Definition 3** (Absolutely maximally entangled states, definition 1 from [23]). *An AME state is a pure state, shared among  $n$  parties  $P = \{1, \dots, n\}$ , each having a system of dimension  $q$ . Hence,  $|\Phi\rangle \in \mathcal{H}_1 \otimes \dots \otimes \mathcal{H}_n$ , with the following equivalent properties:*

- i.  $|\Phi\rangle$  is maximally entangled for any possible bipartition. This means that for any bipartition of  $P$  into disjoint sets  $A$  and  $B$  with  $A \cup B = P$ , and without loss of generality  $m = |B| \leq |A| = n - m$ , the state  $|\Phi\rangle$  can be written in the form:

$$|\Phi\rangle = \frac{1}{\sqrt{d^m}} \sum_{\mathbf{k} \in \mathbb{Z}_q^m} |k_1\rangle_{B_1} |k_2\rangle_{B_2} \dots |k_m\rangle_{B_m} |\phi(\mathbf{k})\rangle_A \quad (1)$$

with  $\langle \phi(k) | \phi(k') \rangle = \delta_{kk'}$

- ii. The reduced density matrix of every subset of parties  $A \subset P$  with  $|A| = \lfloor \frac{n}{2} \rfloor$  is maximally mixed,  $\rho_A = q^{-\lfloor \frac{n}{2} \rfloor} \mathbb{I}_{q^{-\lfloor \frac{n}{2} \rfloor}}$ .
- iii. The reduced density matrix of every subset of parties  $A \subset P$  with  $|A| \leq \frac{n}{2}$  is maximally mixed.
- iv. The von Neumann entropy of every subset of parties  $A \subset P$  with  $|A| = \lfloor \frac{n}{2} \rfloor$  is maximal,  $S(A) = \lfloor \frac{n}{2} \rfloor \log q$ .
- v. The von Neumann entropy of every subset of parties  $A \subset P$  with  $|A| \leq \frac{n}{2}$  is maximal,  $S(A) = |A| \log q$ .

These are all necessary and sufficient conditions for a state to be absolutely maximally entangled. We denote such state as an  $AME(n, q)$  state.

The connection between perfect tensors and AME states was noted in [31], and separately in [15] (where perfect tensors are referred to as multi-unitary matrices). Here we generalise the arguments from [15] to encompass the case of pseudo-perfect tensors.

A  $t$ -index tensor, where each index ranges over  $q$  values, describes a pure quantum state of  $t$   $q$ -dimensional qudits:

$$|\psi\rangle = \sum_{a_1 a_2 \dots a_t \in \mathbb{Z}_q^t} T_{a_1 a_2 \dots a_t} |a_1 a_2 \dots a_t\rangle \quad (2)$$

A necessary and sufficient condition for  $|\psi\rangle$  to be an AME state is that the reduced density matrix of any set of particles  $A$  such that  $|A| \leq \lfloor \frac{t}{2} \rfloor$  is maximally mixed. The reduced density matrix  $\rho_A$  can be calculated as  $\rho_A = M M^\dagger$ , where  $M$  is a  $|A| \times |A^c|$  matrix formed by reshaping  $T$ . Therefore, the state  $|\psi\rangle$  is an AME state if and only if the tensor  $T$  is an isometry from any set of indices  $A$  to the complementary set of indices  $A^c$  with  $|A| \leq |A^c|$ .

If  $t$  is even (odd) this implies that  $T$  is a perfect (pseudo-perfect) tensor. Therefore an AME state containing an even (odd) number of qudits can be described by a perfect (pseudo-perfect) tensor, and every perfect (pseudo-perfect) tensor describes an AME state on an even (odd) number of qudits.

### 3.1.2 (Pseudo-)perfect tensors and quantum error correcting codes

An  $[n, k, d]_q$  quantum error correcting code (QECC) encodes  $k$   $q$ -dimensional qudits into  $n$   $q$ -dimensional qudits, such that  $d - 1$  located errors (or  $\frac{d-1}{2}$  unlocated errors) can be corrected. The quantum Singleton bound states that  $n - k \geq 2(d - 1)$ . A QECC that saturates the quantum Singleton bound is known as a quantum maximum distance separable (MDS) code.

Previous work has established that every  $\text{AME}(2m, q)$  state is the purification of a quantum MDS code [23, 24].<sup>3</sup> Furthermore, viewing the perfect tensor which describes an  $\text{AME}(2m, q)$  state as a linear map from 1 leg to  $2m - 1$  legs, it is the encoding isometry of the quantum MDS code encoding one logical qudit [31].

We can generalise the proof in [24] to further characterise the connection between (pseudo-)perfect tensors and QECC:

**Theorem 3.1.** *Every  $\text{AME}(t, q)$  state is the purification of a  $[t - k, k, \lfloor \frac{t}{2} \rfloor - k + 1]_q$  QECC for  $1 \leq k \leq \lfloor \frac{t}{2} \rfloor$ .*<sup>4</sup>

*Proof.* Let  $|\Phi\rangle$  be an  $\text{AME}(t, q)$  state. For any partition of the state into disjoint sets  $A$  and  $B$  such that  $|A| = \lfloor \frac{t}{2} \rfloor = m$  and  $|B| = \lceil \frac{t}{2} \rceil$  we can write:

$$|\Phi\rangle = \sqrt{\frac{1}{q^m}} \sum_{\mathbf{i} \in \mathbb{Z}_q^m} |i_1 \dots i_m\rangle_A |\phi(\mathbf{i})\rangle_B \quad (3)$$

where  $\langle \phi(\mathbf{i}) | \phi(\mathbf{i}') \rangle = \delta_{\mathbf{i}\mathbf{i}'}$ . If we fix  $k$  qudits to be ‘logical’ qudits, this becomes

$$|\Phi\rangle = \sqrt{\frac{1}{q^m}} \sum_{\mathbf{i} \in \mathbb{Z}_q^k, \mathbf{j} \in \mathbb{Z}_q^{m-k}} |i_1 \dots i_k\rangle_L |j_1 \dots j_{m-k}\rangle_A |\phi(\mathbf{i}, \mathbf{j})\rangle_B \quad (4)$$

where we now have that  $L$  is a fixed set of qudits such that  $|L| = k \leq m$ , and  $A$  and  $B$  are any sets of qudits disjoint from  $L$  and each other such that  $|A| = m - k$ ,  $|B| = \lceil \frac{t}{2} \rceil$ . The set  $A \cup B$  are the physical qudits. Define the basis states of a QECC as:

$$\begin{aligned} |\Phi_{\mathbf{i}}\rangle &= \sqrt{q^k} |i_1 \dots i_k\rangle_L |\Phi\rangle \\ &= \sum_{\mathbf{j} \in \mathbb{Z}_q^{m-k}} \sqrt{\frac{1}{q^{m-k}}} |j_1 \dots j_{m-k}\rangle_A |\phi(\mathbf{i}, \mathbf{j})\rangle_B \end{aligned} \quad (5)$$

Encode a logical state in the physical qudits as:

$$|a\rangle = \sum_{\mathbf{i} \in \mathbb{Z}_q^k} a_{\mathbf{i}} |\Phi_{\mathbf{i}}\rangle \hookrightarrow \sum_{\mathbf{i} \in \mathbb{Z}_q^k} a_{\mathbf{i}} |\Phi_{\mathbf{i}}\rangle \quad (6)$$

Now consider throwing away  $m - k$  of the physical qudits. Since the sets  $A$  and  $B$  in Eq. (6) are arbitrary, we can always choose that the qudits we throw away are in the set  $A$ . The qudits we are left with are then in the state:

$$|\psi\rangle = \sum_{\mathbf{i}, \mathbf{j}} a_{\mathbf{i}} |\phi(\mathbf{i}, \mathbf{j})\rangle_B \quad (7)$$

---

<sup>3</sup>The original proof actually demonstrates that  $\text{AME}(2m, q)$  states are the purification of a threshold quantum secret sharing (QSS) scheme, however every QSS scheme is equivalent to a quantum MDS code [7] so the result follows immediately.

<sup>4</sup>The proof of this theorem is a straightforward generalisation of [24, Theorem 2]

We can recover the logical state by performing the unitary operation:

$$U_B |\phi(\mathbf{i}, \mathbf{j})\rangle_B = \begin{cases} |i_1\rangle_{B_1} \dots |i_k\rangle_{B_{m-k}} |j_1\rangle_{B_{m-k+1}} \dots |j_{m-k}\rangle_{B_m} & \text{for } t \text{ even} \\ |i_1\rangle_{B_1} \dots |i_k\rangle_{B_{m-k}} |j_1\rangle_{B_{m-k+1}} \dots |j_{m-k}\rangle_{B_m} |0\rangle_{B_{m+1}} & \text{for } t \text{ odd} \end{cases} \quad (8)$$

Therefore, any set of  $t - m$  qudits contains all the information about the logical state. By the no-cloning theorem, any set of  $m$  qudits contains no information about the logical state, so the QECC can correct exactly  $m - k = \lfloor \frac{t}{2} \rfloor - k$  erasure errors. This gives  $d = \lfloor \frac{t}{2} \rfloor - k + 1$ .  $\square$

Therefore, an AME( $2m, q$ ) state is the purification of a quantum MDS code with parameters  $[2m - k, k, m - k + 1]_q$ ; while an AME( $2m + 1, q$ ) state is the purification of a QECC with parameters  $[2m + 1 - k, k, m - k + 1]_q$ . The parameters in the AME( $2m + 1, q$ ) case do not saturate the Singleton bound, so it is not an MDS code, but it is an optimal QECC.<sup>5</sup>

If we consider the (pseudo-)perfect tensor,  $T$ , which describes an AME( $t, q$ ) state  $|\Phi\rangle$  we have:

$$|\Phi\rangle = \sum_{\mathbf{i} \in \mathbb{Z}_q^k, \mathbf{j} \in \mathbb{Z}_q^{t-k}} T_{\mathbf{i}, \mathbf{j}} |\mathbf{i}\rangle_L |\mathbf{j}\rangle_P \quad (9)$$

where  $L$  and  $P$  are the sets of logical and physical qudits in the corresponding QECC,  $|L| = k$ ,  $|P| = t - k$ . The basis states for the QECC are then:

$$|\Phi_{\mathbf{i}}\rangle = \sum_{\mathbf{j} \in \mathbb{Z}_q^{t-k}} T_{\mathbf{i}, \mathbf{j}} |\mathbf{j}\rangle_P \quad (10)$$

and the encoding isometry is:

$$V = \sum_{\mathbf{i} \in \mathbb{Z}_q^k, \mathbf{j} \in \mathbb{Z}_q^{t-k}} T_{\mathbf{i}, \mathbf{j}} |\mathbf{j}\rangle \langle \mathbf{i}| \quad (11)$$

So, viewed as an isometry from  $k$  legs to  $t - k$  legs a (pseudo-)perfect tensor is the encoding isometry of a  $[\lfloor \frac{t}{2} \rfloor - k + 1]_q$  QECC.

### 3.1.3 Existence of (pseudo-)perfect tensors

It is possible to construct  $t$ -index (pseudo-)perfect tensors for arbitrarily large  $t$  by increasing  $q$  [2, 16, 23]. In our constructions we are specifically interested in (pseudo-)perfect tensors which describe stabilizer states / codes. These can be constructed for arbitrary  $t$  provided  $q$  is chosen appropriately [22]. A brief outline of the construction is given in Section 3.3.2.

---

<sup>5</sup>The terms MDS quantum code and optimal quantum code are sometimes used interchangeably. Here, by an optimal quantum code we mean either an MDS code, or a code for which  $n - k$  is odd so which cannot saturate the Singleton bound, but for which the distance  $d$  is maximal given this constraint.

### 3.2 Qudit stabilizer codes and states

We restrict our attention to qudits of dimension  $p$  where  $p$  is an odd prime.

#### 3.2.1 Generalised Pauli group

The generalised Pauli operators on  $p$  dimensional qudits are defined as:

$$X = \sum_{j=0}^{p-1} |j+1\rangle\langle j| \quad (12)$$

$$Z = \sum_{j=0}^{p-1} \omega^j |j\rangle\langle j| \quad (13)$$

where  $\omega = e^{\frac{2\pi i}{p}}$ . The generalised Pauli operators obey the relations  $X^p = Z^p = \mathbb{I}$  and  $XZ = \omega ZX$ .

The Pauli group on  $n$  qudits is given by  $\mathcal{G}_{n,p} = \langle \omega^a X^b Z^c \rangle$  where  $a \in \mathbb{Z}_p$ ,  $b, c \in \mathbb{Z}_p^n$ . Two elements  $\omega^a X^b Z^c$  and  $\omega^{a'} X^{b'} Z^{c'}$  commute if and only if  $b' \cdot c = b \cdot c'$ , where all addition is mod  $p$ .

#### 3.2.2 Qudit stabilizer codes

A stabilizer code  $\mathcal{C}$  on  $n$  qudits is a  $p^k$ -dimensional subspace of the Hilbert space given by:

$$\mathcal{C} = \{|\psi\rangle \mid M|\psi\rangle = |\psi\rangle \forall M \in S\} \quad (14)$$

where  $S$  is an Abelian subgroup of  $\mathcal{G}_{n,p}$  that does not contain  $\omega \mathbb{I}$ .

The projector onto  $\mathcal{C}$  is given by [12]:

$$\Pi = \frac{1}{|S|} \sum_{M \in S} M \quad (15)$$

where  $|S| = p^{n-k}$ .  $S$  is an elementary Abelian  $p$ -group, so this implies that a minimal generating set for  $S$  contains  $n-k$  elements.

The minimum weight of a logical operator in an  $[n, k, d]$  stabilizer code is  $d$ . This is also the minimum weight of any operator that is not in the stabilizer, but which commutes with every element of the stabilizer.

#### 3.2.3 Qudit stabilizer codes and (pseudo-)perfect tensors

In Section 3.3 we will see that we can construct (pseudo-)perfect tensors for arbitrary  $t$  such that the AME state described by the tensor is a stabilizer state.<sup>6</sup> This implies, using the method in [13] for generating short qubit stabilizer codes from longer ones, that the QECCs described by the tensors are stabilizer codes:

---

<sup>6</sup>A stabilizer state is a stabilizer code with  $k=0$ .

**Theorem 3.2.** *If a (pseudo-)perfect tensor,  $T$ , with  $t$  legs describes a stabilizer AME( $t, p$ ) state, then the  $[t - k, k, \lfloor \frac{t}{2} \rfloor - k + 1]_p$  QECCs described by the tensor are stabilizer codes. The stabilizers of the code are given by the stabilizers of the AME state which start with  $I^{\otimes k}$ , restricted to the last  $t - k$  qudits.*

*Proof.* Consider an AME( $t, p$ ) stabilizer state with stabilizer  $S$ :

$$|\Phi\rangle = \sqrt{\frac{1}{p^m}} \sum_{\mathbf{i} \in \mathbb{Z}_p^m} |i_1 \dots i_m\rangle_A |\phi(\mathbf{i})\rangle_B \quad (16)$$

where  $|A| = m = \lfloor \frac{t}{2} \rfloor$ ,  $|B| = \lceil \frac{t}{2} \rceil$ .

We have that  $M|\Phi\rangle = |\Phi\rangle$  for all  $M \in S$ , where  $|S| = p^t$  so a minimal generating set for  $S$  contains  $t$  elements. We can always pick a generating set for  $S$  so that  $M_1$  and  $M_2$  begin with  $X$  and  $Z$  respectively, and  $M_3$  to  $M_t$  begin with  $\mathbb{I}$ . Define  $M'_j$  to be  $M_j$  restricted to the last  $t - 1$  qudits, where  $j = 1 : t$ .

Consider the codespace,  $\mathcal{C}$ , for a  $[t - 1, 1, \lfloor \frac{t}{2} \rfloor]_p$  error correcting code described by  $T$ :

$$|\psi\rangle = \sum_{i_1 \in \mathbb{Z}} a_{i_1} |\Phi_{i_1}\rangle \quad (17)$$

where  $\sum_i a_i^2 = 1$  and  $|\Phi_{i_1}\rangle = \sqrt{p} \langle i_1 | \Phi \rangle$ . If we act on  $|\psi\rangle \in \mathcal{C}$  with  $M'_j$  we find  $M'_j |\psi\rangle = |\psi\rangle$  for  $j = 3 : t$ ,  $M'_j |\psi\rangle = |\psi'\rangle \in \mathcal{C}$  where  $|\psi'\rangle \neq |\psi\rangle$  for  $j = 1 : 2$ .

The group  $S'$  generated by  $M'_j$  for  $j = 3 : t$  contains  $|S'| = p^{t-2}$  elements, and it stabilizes the  $[t - 1, 1, \lfloor \frac{t}{2} \rfloor]_p$  code. We can carry out a similar procedure starting from the  $[t - 1, 1, \lfloor \frac{t}{2} \rfloor]_p$  code, and removing more stabilizer generators to obtain the other QECC.  $\square$

We refer to (pseudo-)perfect tensors which describe stabilizer AME states (and therefore stabilizer QECC) as stabilizer (pseudo-)perfect tensors.

We also require that all the QECC used in our construction map logical Pauli operators to physical Pauli operators. It is known that for qubit stabilizer codes a basis can always be chosen so that this is true [13], and the same group-theoretic proof applies to qudit stabilizer codes.<sup>7</sup> The physical Pauli operators we obtain using this method are not given by acting on the logical Pauli operators with the encoding isometry, but they have the same action in the code subspace. So, we have that for qudit stabilizer codes it is always possible to pick a basis where  $V P V^\dagger = P' V V^\dagger$  where  $P$

<sup>7</sup>The discussion in [13] actually shows that there is an automorphism between  $\mathcal{G}_{k,2}$  and  $N(S)/S$ , where  $N(S)$  is the normalizer of  $S$  in  $\mathcal{G}_{n,2}$ . As  $N(S) \in \mathcal{G}_{n,2}$  this is sufficient. The discussion in [13] can be extended to qudits of prime dimension by replacing phase factors of 4 with factors of  $p$ , and dimension factors of 2 with factors of  $p$ .

is a  $k$ -qudit Pauli operator,  $P'$  is an  $n$ -qudit Pauli operator, and  $V$  is the encoding isometry of the QECC.

In our holographic QECC we do not have complete freedom to pick a basis, so we also need to show that we can pick this basis consistently. In order to show this we will require two lemmas about qudit stabilizer codes.

**Lemma 3.3.** *The smallest subgroup,  $G$ , of the Pauli group  $\mathcal{G}_{n,p}$  such that  $\forall P \in \mathcal{G}_{n,p}, P \neq \mathbb{I}^{\otimes n}, \exists M \in G$  where  $MP \neq PM$  is the entire Pauli group.*

*Proof.* Consider the following process for constructing a set  $A$  element by element such that  $\forall P \in \mathcal{G}_{n,p}, P \neq \mathbb{I}^{\otimes n}, \exists M \in A$  where  $MP \neq PM$ :

1. Select an arbitrary element of  $\mathcal{G}_{n,p}$ ,  $P^{(1)} = \omega^{a^{(1)}} X^{\mathbf{b}^{(1)}} Z^{\mathbf{c}^{(1)}}$ .
2. Pick an element  $P^{(1')} = \omega^{a^{(1')}} X^{\mathbf{b}^{(1')}} Z^{\mathbf{c}^{(1')}}$  such that  $\mathbf{b}^{(1')} \cdot \mathbf{c}^{(1)} \neq \mathbf{b}^{(1)} \cdot \mathbf{c}^{(1')}$ . This ensures that  $P^{(1')}$  does not commute with  $P^{(1)}$ , and  $P^{(1')}$  is our first element of  $A$ .
3. Pick an arbitrary element,  $P^{(i)}$  of  $\mathcal{G}_{n,p}$  which commutes with every element of  $A$  and is not the identity.
4. Choose any element,  $P^{(i')}$  of  $\mathcal{G}_{n,p}$  which does not commute with  $P^{(i)}$ , and add it to  $A$ .
5. Repeat steps (3) and (4) until  $\forall P \in \mathcal{G}_{n,p}, P \neq \mathbb{I}^{\otimes n}, \exists M \in A$  such that  $MP \neq PM$ .

When we construct  $A$ , every element  $P^{(i')} = \omega^{a^{(i')}} X^{\mathbf{b}^{(i')}} Z^{\mathbf{c}^{(i')}}$  which we add to  $A$  is independent from every element already in  $A$ . To see this note that by assumption there is some  $P^{(i)}$  which commutes with every element in  $A$ , but does not commute with  $P^{(i')}$ . If  $P^{(i')}$  was not independent from the other elements of  $A$ , and  $\mathbf{b}^{(i')} = \mathbf{b}^{(1')} + \mathbf{b}^{(2')}$  and  $\mathbf{c}^{(i')} = \mathbf{c}^{(1')} + \mathbf{c}^{(2')}$  where  $P^{(1')}, P^{(2')} \in A$  then  $\mathbf{b}^{(i')} \cdot \mathbf{c}^{(i)} = \mathbf{b}^{(1')} \cdot \mathbf{c}^{(i)} + \mathbf{b}^{(2')} \cdot \mathbf{c}^{(i)} = \mathbf{b}^{(i)} \cdot \mathbf{c}^{(1')} + \mathbf{b}^{(i)} \cdot \mathbf{c}^{(2')}$  and  $\mathbf{b}^{(i)} \cdot \mathbf{c}^{(i')} = \mathbf{b}^{(i)} \cdot \mathbf{c}^{(1')} + \mathbf{b}^{(i)} \cdot \mathbf{c}^{(2')}$  so  $\mathbf{b}^{(i')} \cdot \mathbf{c}^{(i)} = \mathbf{b}^{(i)} \cdot \mathbf{c}^{(i')}$ , and  $P^{(i')}$  would commute with  $P^{(i)}$ , contradicting our initial assumption.

We need to determine the minimum number of elements in  $A$  when this process terminates.

Suppose we have repeated steps (3) and (4)  $m$  times, so that  $|A| = m$ . If there is an element  $P^{(k)} = \omega^{a^{(k)}} X^{\mathbf{b}^{(k)}} Z^{\mathbf{c}^{(k)}}$  of  $\mathcal{G}_{n,p}$  which commutes with every element of  $A$  then  $\mathbf{b}^{(i')} \cdot \mathbf{c}^{(k)} = \mathbf{b}^{(k)} \cdot \mathbf{c}^{(i')}$  for all  $P^{(i')} \in A$ .  $P^{(k)}$  is described by  $2n$  degrees of freedom:  $b_1^{(k)}, \dots, b_n^{(k)}$  and  $c_1^{(k)}, \dots, c_n^{(k)}$ , and there are  $m$  homogeneous equations which  $P^{(k)}$  needs to satisfy.<sup>8</sup> Provided  $m < 2n$ , the set of equations is underdetermined, and we can always choose a  $P^{(k)}$

---

<sup>8</sup>The equations are homogeneous as all constant terms are equal to zero. Homogeneity of the equations ensures that the equations are not inconsistent.

which commutes with every element of  $A$  and is not the identity. If  $m = 2n$  then the solution to the equations is uniquely determined, and is the identity. At this point we cannot continue with the process, so it terminates with  $|A| = 2n$ .

Therefore, the smallest set  $A$  of elements of  $\mathcal{G}_{n,p}$  such that  $\forall P \in \mathcal{G}_{n,p}$ ,  $P \neq \mathbb{I}^{\otimes n}$ ,  $\exists M \in A$  where  $MP \neq PM$  contains  $2n$  elements. At this stage  $A$  is not a group because all the elements of  $A$  are independent so the set isn't closed. Any  $2n$  independent elements of  $\mathcal{G}_{n,p}$  generate the entire group, so the smallest group  $G$  which contains every element of  $A$  is  $\mathcal{G}_{n,p}$  itself.  $\square$

**Lemma 3.4.** *In an  $[n, k, d]_p$  stabilizer code, the action of an encoded Pauli operator  $\overline{P}$  on any  $d - 1$  physical qudits can be chosen to be any element of  $\mathcal{G}_{d-1,p}$ .*

*Proof.* The encoded Pauli operator  $\overline{P}$  is not unique, and the different possible physical operators are related by elements of the stabilizer. We therefore need to show that the stabilizer  $S$  restricted to any set of  $d - 1$  qudits is the entire Pauli group  $\mathcal{G}_{d-1,p}$ .

An  $[n, k, d]_p$  stabilizer code can correct all Pauli errors of weight  $d - 1$  and less. A correctable error doesn't commute with some element of the stabilizer, so for any Pauli operator of weight  $d - 1$  there  $\exists M \in S$  such that  $[M, P] \neq 0$ . The result follows immediately from Lemma 3.3.  $\square$

**Theorem 3.5.** *If there exists a basis such that the QECC described by a (pseudo-)perfect tensor,  $T$ , from qudit  $l$  to  $t - 1$  qudits maps Pauli operators to Pauli operators, then all other QECC described by  $T$  which include qudit  $l$  in the logical set also map Pauli operators to Pauli operators in that basis.*

*Proof.* Let the AME state described by  $T$  be given by:

$$|\Phi\rangle = \sum_{a \in \mathbb{Z}_p} \sum_{\mathbf{b} \in \mathbb{Z}_p^{k-1}} \sum_{\mathbf{c} \in \mathbb{Z}_p^{m-k}} |a\rangle_l |b_1 \dots b_{k-1}\rangle_L |c_1 \dots c_{m-k}\rangle_A |\phi(a, \mathbf{b}, \mathbf{c})\rangle_B \quad (18)$$

where  $m = \lfloor \frac{t}{2} \rfloor$ , and  $|B| = \lceil \frac{t}{2} \rceil$ .

The basis states of the  $[t - 1, 1, \lfloor \frac{t}{2} \rfloor]_p$  QECC from qudit  $l$  to other  $t - 1$  qudits are given by:

$$|\Phi_a\rangle = \sum_{\mathbf{b} \in \mathbb{Z}_p^{k-1}} \sum_{\mathbf{c} \in \mathbb{Z}_p^{m-k}} |b_1 \dots b_{k-1}\rangle_L |c_1 \dots c_{m-k}\rangle_A |\phi(a, \mathbf{b}, \mathbf{c})\rangle_B \quad (19)$$

and the encoding isometry is given by:

$$V = \sum_a |\Phi_a\rangle \langle a| \quad (20)$$

The basis states of a  $[t - k, k, \lfloor \frac{t}{2} \rfloor - k + 1]_p$  QECC from a set  $L$  qudits (where  $l \in L, |L| = k$ ) to  $t - k$  qudits is given by:

$$|\Phi_{a,b}\rangle = \sum_{\mathbf{c} \in \mathbb{Z}_p^{m-k}} |c_1 \dots c_{m-k}\rangle_A |\phi(a, \mathbf{b}, \mathbf{c})\rangle_B \quad (21)$$

and the encoding isometry is given by:

$$V' = \sum_a |\Phi_{a,b}\rangle \langle a, \mathbf{b}| \quad (22)$$

By assumption we have:

$$VP_1V^\dagger = QVV^\dagger \quad (23)$$

where  $P_1 \in \mathcal{G}_{1,p}$  and  $Q \in \mathcal{G}_{n,p}$ ,  $n = t - 1$ .

Therefore:

$$\sum_{aa'} |\Phi_a\rangle \langle a| P_1 |a'\rangle \langle \Phi_{a'}| = Q \sum_a |\Phi_a\rangle \langle \Phi_a| \quad (24)$$

Consider the action of  $V'$  on  $P_1 \otimes P_2 \in \mathcal{G}_{k,p}$ :

$$\begin{aligned} V'(P_1 \otimes P_2)V'^\dagger &= \sum_{a,a',\mathbf{b},\mathbf{b}'} |\Phi_{a,b}\rangle \langle a, \mathbf{b}| (P_1 \otimes P_2) |a, \mathbf{b}\rangle \langle \Phi_{a,b}| \\ &= \sum_{a,a',\mathbf{b},\mathbf{b}'} \langle \mathbf{b} | \Phi_a \rangle \langle a | P_1 | a' \rangle \langle \mathbf{b} | P_2 | \mathbf{b}' \rangle \langle \Phi_{a'} | \mathbf{b}' \rangle \\ &= \sum_{a,a',\mathbf{b},\mathbf{b}'} \langle \mathbf{b} | P_2 | \mathbf{b}' \rangle \langle \mathbf{b} | (|\Phi_a\rangle \langle a| P_1 |a'\rangle \langle \Phi_{a'}|) | \mathbf{b}' \rangle \\ &= \sum_{a,\mathbf{b},\mathbf{b}'} \langle \mathbf{b} | P_2 | \mathbf{b}' \rangle \langle \mathbf{b} | (Q |\Phi_a\rangle \langle \Phi_a|) | \mathbf{b}' \rangle \quad (25) \\ &= \sum_{a,\mathbf{b},\mathbf{b}',\mathbf{b}''} \langle \mathbf{b} | P_2 | \mathbf{b}' \rangle \langle \mathbf{b} | Q'_2 | \mathbf{b}'' \rangle Q' |\Phi_{a,b''}\rangle \langle \Phi_{a,b'}| \\ &= \sum_{a,\mathbf{b}} Q' |\Phi_{a,b}\rangle \langle \Phi_{a,b}| \text{ if } P_2 = Q'_2 \\ &= V'V'^\dagger P'^{(n')} \end{aligned}$$

where and  $Q'_2$  and  $Q'$  indicate  $Q$  restricted to the first  $k - 1$  and remaining  $n - k - 1$  qudits respectively ( $Q = Q'_2 \otimes Q'$ ).

Therefore, if  $Q$  acts as  $P_2$  on the first  $k - 1$  qudits, then  $P_1 \otimes P_2$  maps to a Pauli under  $V'$ . The operator  $Q$  is not unique, and from Lemma 3.4 we know that its action on  $\lfloor \frac{t}{2} \rfloor - 1$  qudits can be chosen to be any element of  $\mathcal{G}_{\lfloor \frac{t}{2} \rfloor - 1, p}$ . So we can choose that  $Q$  acts as  $P_2$  on the first  $k - 1$  qudits, for  $k \leq \lfloor \frac{t}{2} \rfloor$ .  $\square$

### 3.3 Existence of (pseudo-)perfect stabilizer tensors

#### 3.3.1 Classical coding theory

A classical linear  $[n, k]_d$  code,  $\mathcal{C}_{cl}$ , encodes  $k$   $d$ -dimensional dits of information in  $n$  dits. It can be described by a generator matrix  $G^T : \mathbb{Z}_p^k \rightarrow \mathbb{Z}_d^n$ , where information is encoded as  $\mathbf{x} \hookrightarrow G^T \mathbf{x}$  for  $\mathbf{x} \in \mathbb{Z}_d^k$ . Equivalently,  $\mathcal{C}_{cl}$  admits a description as the kernel of a parity check matrix  $H : \mathbb{Z}_d^n \rightarrow \mathbb{Z}_d^{n-k}$ . Consistency of the two descriptions implies  $HG^T \mathbf{x} = 0, \forall \mathbf{x} \in \mathbb{Z}_d^k$ , and hence the rows of  $H$  are orthogonal to the rows of  $G$ .

The minimum distance  $\delta$  of a classical code is defined as the minimum Hamming distance between any two code words. It is bounded by the classical Singleton bound,  $\delta \leq n - k + 1$ . Codes which saturate the classical Singleton bound are referred to as classical MDS codes.

Reed-Solomon codes are a class of classical MDS codes [34].<sup>9</sup>

**Definition 4.** Let  $p$  be a prime, and let  $k, n$  be integers such that  $k < n \leq p$ . For a set  $S = \{\alpha_1, \alpha_2, \dots, \alpha_n\} \in \mathbb{Z}_p$ , the Reed-Solomon code over  $\mathbb{Z}_p$  is defined as:

$$\mathcal{C}_{RS}[n, k] = \{(P(\alpha_1), P(\alpha_2), \dots, P(\alpha_n)) \in \mathbb{Z}_p^n \mid P(X) \in \mathbb{Z}_p[X], \deg(P) \leq k-1\} \quad (26)$$

where  $\mathbb{Z}_p[X]$  is the polynomial ring in  $X$  over  $\mathbb{Z}_p$ .<sup>10</sup>

To encode a message  $\mathbf{a} = (a_0, a_1, \dots, a_{k-1}) \in \mathbb{Z}_p^k$  in the Reed-Solomon code define the polynomial:

$$P_{\mathbf{a}}(X) = a_0 + a_1 X + a_2 X^2 + \dots + a_{k-1} X^{k-1} \quad (27)$$

and construct the codeword  $(P_{\mathbf{a}}(\alpha_1), P_{\mathbf{a}}(\alpha_2), \dots, P_{\mathbf{a}}(\alpha_n)) \in \mathcal{C}_{RS}[n, k]$ .

Reed-Solomon codes are linear codes, with generating matrix:

$$G = \begin{pmatrix} 1 & 1 & 1 & \dots & 1 \\ \alpha_1 & \alpha_2 & \alpha_3 & \dots & \alpha_n \\ \alpha_1^2 & \alpha_2^2 & \alpha_3^2 & \dots & \alpha_n^2 \\ \vdots & \vdots & \vdots & \ddots & \vdots \\ \alpha_1^{k-1} & \alpha_2^{k-1} & \alpha_3^{k-1} & \dots & \alpha_n^{k-1} \end{pmatrix} \quad (28)$$

The generator matrix can be put into standard form  $G = [I_k | P]$  (where  $P$  is a  $k \times (n - k)$  matrix) using Gauss-Jordan elimination over the field  $\mathbb{Z}_p$ . The parity check matrix is then given by  $H = [P^T | I_{n-k}]$ .

<sup>9</sup>Reed Solomon codes can be defined over any finite field, but we only require the definition of Reed Solomon codes over  $\mathbb{Z}_p$  for our construction.

<sup>10</sup>The polynomial ring in  $X$  over  $\mathbb{Z}_p$ ,  $\mathbb{Z}_p[X]$ , is the set of polynomials  $P(X) = a_0 + a_1 X + a_2 X^2 + \dots + a_m X^m$  where  $a_i \in \mathbb{Z}_p$ .

### 3.3.2 Constructing AME stabilizer states

An AME( $t, p$ ) stabilizer state  $|\Phi\rangle$  can be constructed from a classical  $[t, \lfloor \frac{t}{2} \rfloor]_p$  MDS code with  $\delta = \lceil \frac{t}{2} \rceil + 1$ . The state is given by [22]:

$$|\Phi\rangle = \frac{1}{d^{\frac{t}{2}}} \sum_{\mathbf{x} \in \mathbb{Z}_p^t} |G\mathbf{x}\rangle \quad (29)$$

and has stabilizers  $X^{G\mathbf{y}}$  for all  $\mathbf{y} \in \mathbb{Z}_p^t$ , and  $Z^{\mathbf{y}}$  where  $\mathbf{y}^T = \mathbf{z}^T H$  for all  $\mathbf{z} \in \mathbb{Z}_p^m$ . The full set of stabilizers is given by the generator matrix [22]:

$$M = \left( \begin{array}{c|c} G & 0 \\ 0 & H \end{array} \right) \quad (30)$$

where  $(\alpha | \beta) \equiv X^\alpha \cdot Z^\beta$  for  $\alpha, \beta \in \mathbb{Z}_p^t$ .

Reed-Solomon codes can be constructed for any  $k, n$  satisfying  $k < n \leq p$  [34], so by increasing  $p$  this construction can provide AME( $t, p$ ) stabilizer states for arbitrarily large  $t$ . By Theorem 3.2 the tensor which describes the AME( $t, p$ ) stabilizer states will be a stabilizer (pseudo-)perfect tensor.

This construction is not optimised to minimise  $p$  for a given  $t$ . It is possible to construct generalised Reed-Solomon codes which exist for  $n = p+1$  [37], which if used in this construction will give (pseudo-)perfect stabilizer tensors acting on lower dimensional qudits for certain values of  $t$ . There are also methods for constructing stabilizer perfect tensors for which  $p \propto \sqrt{t}$  using cyclic and constacyclic classical MDS codes [17], but this method is significantly more involved than the one presented here, and does not work for pseudo-perfect tensors. In our construction there is no benefit to minimising  $p$ , so we have selected the simplest, most universal method for constructing (pseudo-)perfect stabilizer tensors.

## 3.4 Hyperbolic Coxeter groups

### 3.4.1 Coxeter systems

The holographic error correcting codes presented in this paper are tensor networks embedded in tessellations of  $\mathbb{H}^3$ . We will use Coxeter systems to analyse these tessellations.<sup>11</sup>

**Definition 5** (Coxeter system [40]). *Let  $S = \{s_i\}_{i \in I}$ , be a finite set. Let  $M = (m_{i,j})_{i,j \in I}$  be a matrix such that:*

- $m_{ii} = 1, \forall i \in I$
- $m_{ij} = m_{ji}, \forall i, j \in I, i \neq j$
- $m_{ij} \in (\mathbb{N} \setminus \{1\}) \cup \{\infty\}, \forall i, j \in I, i \neq j$

---

<sup>11</sup>An overview of hyperbolic Coxeter groups can be found at [11].

$M$  is called the Coxeter matrix. The associated Coxeter group,  $W$ , is defined by the presentation:<sup>12</sup>

$$W = \langle S \mid (s_i s_j)^{m_{ij}} = 1 \forall i, j \in I \rangle \quad (31)$$

The pair  $(W, S)$  is called a Coxeter system.

To understand the connection between Coxeter systems and tessellations of hyperbolic space we need to introduce the notion of a Coxeter polytope.

**Definition 6.** A convex polytope in  $\mathbb{X}^d = \mathbb{S}^d, \mathbb{E}^d$  or  $\mathbb{H}^d$  is a convex intersection of a finite number of half spaces. A Coxeter polytope  $P \subseteq \mathbb{X}^d$  is a polytope with all dihedral angles integer submultiples of  $\pi$ .

A Coxeter system can be associated to every Coxeter polytope. Let  $(F_i)_{i \in I}$  be the facets of  $P$ , and if  $F_i \cap F_j \neq \emptyset$  set  $m_{ij} = \frac{\pi}{\alpha_{ij}}$ , where  $\alpha_{ij}$  is the dihedral angle between facets  $F_i$  and  $F_j$ . Set  $m_{ii} = 1$ , and if  $F_i \cap F_j = \emptyset$  set  $m_{ij} = \infty$ . Let  $s_i$  be the reflection in  $F_i$ . The Coxeter group with Coxeter matrix  $(m_{ij})_{i,j \in I}$  is a discrete subgroup of  $\text{Isom}(\mathbb{X}^d)$ , generated by reflections in the facets of  $P$ , and  $P$  tiles  $\mathbb{X}^d$  [10].

Coxeter systems can be represented by Coxeter diagrams. In a Coxeter diagram a vertex is associated to every  $s_i$  (or equivalently to every facet in the corresponding Coxeter polytope). Vertices are connected by edges in the following manner:

- If  $m_{ij} = 2$  (i.e. facets  $F_i$  and  $F_j$  in the Coxeter polytope are orthogonal) there is no edge between the vertices representing  $s_i$  and  $s_j$
- If  $m_{ij} = 3$  (i.e. the dihedral angle between  $F_i$  and  $F_j$  is  $\frac{\pi}{3}$ ) there is an unlabelled edge between vertices representing  $s_i$  and  $s_j$
- If  $m_{ij} \in \mathbb{N} \setminus \{1, 2, 3\}$  (i.e. the dihedral angle between  $F_i$  and  $F_j$  is  $\frac{\pi}{m_{ij}}$ ) there is an edge labelled with  $m_{ij}$  between vertices representing  $s_i$  and  $s_j$
- If  $m_{ij} = \infty$  (i.e. facets  $F_i$  and  $F_j$  in the Coxeter polytope diverge) there is a dashed edge between the vertices representing  $s_i$  and  $s_j$

A Coxeter group is irreducible if its Coxeter diagram is connected.

Faces of  $P$  correspond to subsets of  $S$  that generate finite Coxeter groups:<sup>13</sup>

**Lemma 3.6** (From [41]).  $f = \cup_{i \in I} F_i$  is a codimension  $|I|$  face of  $P$  if and only if  $\{s_i \mid i \in I\}$  generates a finite Coxeter group.

<sup>12</sup>A group presentation  $\langle S \mid R \rangle$ , where  $S$  is a set of generators and  $R$  is a set of relations between the generators, defines a group which is (informally) the largest group which is generated by  $S$  and in which all the relations in  $R$  hold.

<sup>13</sup>This does not apply to ideal vertices (vertices at the boundary of  $\mathbb{X}^d$ ) however in this paper we are only concerned with compact polyhedra, which do not have vertices at infinity.

### 3.4.2 Combinatorics of Coxeter groups

A lot of research has been carried out into the combinatorics of Coxeter groups. Here we briefly introduce the notions which we later use to prove properties of our holographic error correcting code.

Let  $(W, S)$  be a Coxeter system. Every element  $w \in W$  can be written as a product of generators:

$$w = s_1 s_2 \dots s_k \text{ for } s_i \in S \quad (32)$$

This description is not unique. We can define a length function with respect to the generating set  $S$ . The length of the identity element is defined as  $l_S(1) = 0$ , and the length of a non-trivial element of the Coxeter group is given by:

$$l_S(w) = \min\{l \in \mathbb{N} \mid s_1 s_2 \dots s_l = w\} \quad (33)$$

An expression for  $w$  with the minimum number of generators,  $s_1 s_2 \dots s_{l_S(w)}$  is called a reduced word for  $w$ .

Coxeter groups satisfy the Deletion Condition:

**Definition 7** (Deletion Condition). *Let  $(W, S)$  be a pair where  $W$  is a group and  $S$  is a generating set for  $W$  consisting entirely of elements of order two. We say that this pair satisfies the Deletion Condition if for any non reduced word  $s_1 \dots s_r$  over  $S$  there are two indices  $i$  and  $j$  such that:*

$$s_1 \dots s_r =_w s_1 \dots \hat{s}_i \dots \hat{s}_j \dots s_r \quad (34)$$

where the carets indicate omission.

The length function on Coxeter groups has a number of important properties:

- (i)  $l_S(ws) = l_S(w) \pm 1$  for all  $s \in S$
- (ii)  $l_S(sw) = l_S(w) \pm 1$  for all  $s \in S$
- (iii)  $l_S(w^{-1}) = l_S(w)$  for all  $w \in W$
- (iv)  $|l_S(u) - l_S(w)| \leq l_S(uw) \leq l_S(u) + l_S(w)$  for all  $u, w \in W$
- (v)  $d(u, w) = l_S(u^{-1}w)$  for  $u, w \in W$  is a metric on  $W$  (referred to as the word metric)

By conditions (i) and (ii), if we define the following sets:

$$\begin{aligned} \mathcal{D}_R(w) &= \{s \in S \mid l_S(ws) = l_S(w) - 1\} \\ \mathcal{A}_R(w) &= \{s \in S \mid l_S(ws) = l_S(w) + 1\} \\ \mathcal{D}_L(w) &= \{s \in S \mid l_S(sw) = l_S(w) - 1\} \\ \mathcal{A}_L(w) &= \{s \in S \mid l_S(sw) = l_S(w) + 1\} \end{aligned} \quad (35)$$

then we have  $\mathcal{D}_R(w) \cup \mathcal{A}_R(w) = \mathcal{D}_L(w) \cup \mathcal{A}_L(w) = S$  and  $\mathcal{D}_R(w) \cap \mathcal{A}_R(w) = \mathcal{D}_L(w) \cap \mathcal{A}_L(w) = \{\}$ . We refer to  $\mathcal{D}_R(w)$  and  $\mathcal{D}_L(w)$  ( $\mathcal{A}_R(w)$ ,  $\mathcal{A}_L(w)$ ) as the right and left descent sets (ascent sets) of  $w$  respectively.

**Lemma 3.7** (Corollary 2.18 from [1]). *For all  $w \in W$ , the Coxeter groups generated by  $\mathcal{D}_R(w)$  and  $\mathcal{D}_L(w)$  are finite.*<sup>14</sup>

The irreducible finite Coxeter groups are classified in Table 1. A general Coxeter group is finite if and only if each connected component of the Coxeter graph generates a finite Coxeter group.

Finally, we note that if  $s \in \mathcal{D}_R(w)$  ( $s \in \mathcal{D}_L(w)$ ) there is a reduced word for  $w$  that ends in  $s$  (begins with  $s$ ).

### 3.4.3 Growth rates of Coxeter groups

The growth series of a Coxeter group with respect to a set of generators  $S$  is defined as:

$$f_S(x) = \sum_{w \in W} x^{l_S(w)} = 1 + Sx + \dots = 1 + \sum_{i \geq 1} a_i x^i \quad (36)$$

where  $a_i$  is the number of  $w \in W$  satisfying  $l_S(w) = i$ . The growth rate is given by:

$$\tau = \limsup_{n \rightarrow \infty} \sqrt[n]{a_n} \quad (37)$$

Spherical and Euclidean Coxeter groups have growth rate 0 and 1 respectively. Hyperbolic Coxeter groups have  $\tau > 1$ .

### 3.4.4 Coxeter groups in $\mathbb{H}^3$

We will be interested in compact Coxeter polytopes in hyperbolic 3-space,  $\mathbb{H}^3$ , and their associated Coxeter systems. Andreev's theorem provides a classification of such polytopes:

**Theorem 3.8** (Andreev's theorem, from [4]). *A compact acute-angled polytope  $P$  of a given simple combinatorial type with given dihedral angles exists in  $\mathbb{H}^3$  exists if and only if the following conditions holds:*

1. *if three faces  $F_i, F_j, F_k$  pass through the same vertex then  $\alpha_{ij} + \alpha_{jk} + \alpha_{ki} > \pi$ ;*
2. *if the faces  $F_i, F_j, F_k$  form a three circuit then  $\alpha_{ij} + \alpha_{jk} + \alpha_{ki} < \pi$ , where faces form a  $k$ -circuit if  $F_i$  shares a common edge with  $F_{i+1}$  for  $i = 1 \dots k$  where  $F_{k+1} = F_1$ ;*
3. *if the faces  $F_i, F_j, F_k, F_l$  form a four circuit then  $\alpha_{ij} + \alpha_{jk} + \alpha_{kl} + \alpha_{li} < 2\pi$ ;*

---

<sup>14</sup>All subsets of  $S$  generate a Coxeter group.

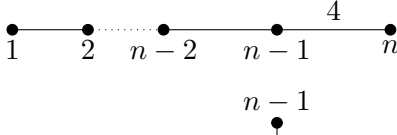
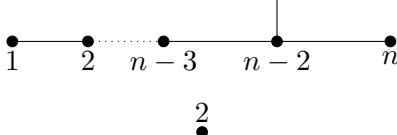
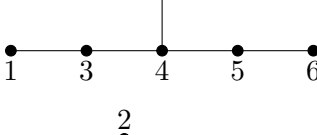
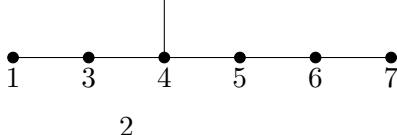
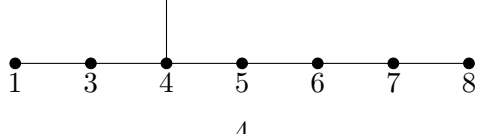
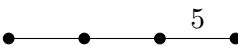
Name	Coxeter diagram
$A_n$ ( $n \geq 1$ )	
$B_n = C_n$ ( $n \geq 3$ )	
$D_n$ ( $n \geq 4$ )	
$E_6$	
$E_7$	
$E_8$	
$F_4$	
$G_2$	
$H_3$	
$H_4$	
$I_2^{(m)}$ ( $m \geq 3$ )	

Table 1: Diagrams of irreducible finite Coxeter systems. Table reproduced from [8].

4. if  $P$  is a triangular prism then at least one dihedral angle between a triangular side and a quadrilateral side is not equal to  $\frac{\pi}{2}$
5. if  $P$  is a tetrahedon then the determinant of the Gram matrix should be negative

For a given Coxeter diagram it is straightforward to check whether the associated Coxeter polytope meets the conditions of Andreev's theorem, and therefore whether the Coxeter polytope tiles  $\mathbb{H}^3$ .

### 3.5 Hamiltonian simulation

#### 3.5.1 Hamiltonian encodings

In [9] it is shown that if an encoding  $H' = \mathcal{E}(H)$  has the following three properties:

1.  $\mathcal{E}(A) = \mathcal{E}(A)^\dagger$  for all  $A \in \text{Herm}_n$
2.  $\text{spec}(\mathcal{E}(A)) = \text{spec}(A)$  for all  $A \in \text{Herm}_n$
3.  $\mathcal{E}(pA + (1-p)B) = p\mathcal{E}(A) + (1-p)\mathcal{E}(B)$  for all  $A, B \in \text{Herm}_n$  and all  $p \in [0, 1]$

then it must be of the form:

$$\mathcal{E}(M) = U(M \otimes P = \overline{M} \otimes Q)U^\dagger \quad (38)$$

for orthogonal projectors  $P, Q$  such that  $P + Q = \mathbb{I}$  where  $U$  is a unitary, and  $\overline{M}$  denotes complex conjugation.

Furthermore, it is shown that under any such encoding,  $H'$  will reproduce all the static, dynamic, and thermodynamic properties of  $H$ .

If the encoding  $\mathcal{E}(H)$  only acts within a subspace of the simulator system  $\mathcal{H}'$  then the unitary  $U$  is replaced with an isometry  $W$ :

$$\mathcal{E}(M) = W(M \otimes P = \overline{M} \otimes Q)W^\dagger \quad (39)$$

The stabilizer codes discussed in Section 3.2.2 are an example of subspace encodings with the particularly simple structure,  $\mathcal{E}(M) = WMW^\dagger$ .

A local encoding is an encoding which maps local observables to local observables.

**Definition 8** (Local encoding into a subspace (this is a generalisation of definition 13 from [9]). *Let  $\mathcal{E} : \mathcal{B}(\otimes_{i=1}^n \mathcal{H}_i) \rightarrow \mathcal{B}(\otimes_{i=1}^{n'} \mathcal{H}'_i)$  be a subspace encoding, and let  $\{S'_i\}_{i=1}^n$  be subsets of  $[n']$ . We say that  $\mathcal{E}$  is local with respect to  $\{S'_i\}$  if for any operator  $A_i \in \text{Herm}(\mathcal{H}_i)$  there exists  $A'_i \in \text{Herm}(\otimes_{i=1}^{n'} \mathcal{H}'_i)$  which acts non-trivially only on  $\{S'_i\}$  such that:*

$$\mathcal{E}(A_i \otimes \mathbb{I}) = (A'_i \otimes \mathbb{I})\mathcal{E}(\mathbb{I}) \quad (40)$$

### 3.5.2 Hamiltonian simulation

We say Hamiltonian  $H'$  perfectly simulates Hamiltonian  $H$  if  $H'$  reproduces the physics of  $H$  below some energy cut-off  $\Delta$ , where  $\Delta$  can be made arbitrarily large.

**Definition 9** (Exact simulation, definition 20 from [9]). *We say that  $H'$  perfectly simulates  $H$  below energy  $\Delta$  if there is a local encoding  $\mathcal{E}$  into the subspace  $S_{\mathcal{E}}$  such that*

- i.  $S_{\mathcal{E}} = S_{\leq \Delta(H')}$  (or equivalently  $\mathcal{E}(\mathbb{I}) = P_{\leq \Delta(H')}$ )
- ii.  $H'|_{\leq \Delta} = \mathcal{E}(H)|_{S_{\mathcal{E}}}$

If  $\mathcal{E}(M) = WMW^{\dagger}$  is an encoding where  $W$  is the encoding isometry of some stabilizer code and  $\Pi = WW^{\dagger}$  is the projector onto the code-space, then  $H' = \mathcal{E}(H) + \Delta\Pi$  simulates  $H$  below energy  $\Delta$ .

We can also consider the case where the simulation is only approximate:

**Definition 10** (Approximate simulation, definition 23 from [9]). *We say that  $H'$  is a  $(\Delta, \eta, \epsilon)$ -simulation of  $H$  if there exists a local encoding  $\mathcal{E}(M) = W(M \otimes P + \overline{M} \otimes Q)W^{\dagger}$  such that:*

- i. There exists an encoding  $\tilde{\mathcal{E}}(M) = \tilde{W}(M \otimes P + \overline{M} \otimes Q)\tilde{W}^{\dagger}$  such that  $S_{\tilde{\mathcal{E}}} = S_{\leq \Delta(H')}$  and  $\|W - \tilde{W}\| \leq \eta$ ;
- ii.  $\|H'_{\leq \Delta} - \tilde{\mathcal{E}}(H)\| \leq \epsilon$

### 3.5.3 Perturbation gadgets

In this section we collect some results regarding perturbative techniques, and introduce some new qudit perturbation gadgets which are used in this paper.

Consider an unperturbed Hamiltonian  $H$ , with degenerate ground space of energy zero, and a spectral gap above the ground space of  $\Delta$ . Let  $\tilde{H} = H + V$  where  $V$  is some perturbation. Decompose the Hilbert space as  $\mathcal{H} = \mathcal{H}_- \oplus \mathcal{H}_+$  where  $\mathcal{H}_-$  is the ground space of  $H$ . Let  $\Pi_{\pm}$  be the projectors onto  $\mathcal{H}_{\pm}$ . For arbitrary operator  $M$  define  $M_{++} = \Pi_+ M \Pi_+$ ,  $M_{--} = \Pi_- M \Pi_-$ ,  $M_{+-} = \Pi_+ M \Pi_-$ , and  $M_{-+} = \Pi_- M \Pi_+$ .

The self energy is defined as:

$$\Sigma_-(z) = H_- + V_{--} + V_{-+}G_+ (I_+ - V_{++}G_+)^{-1} V_{+-} \quad (41)$$

where  $G_+$  is the unperturbed Greens function, defined by:

$$G_+^{-1} = zI_+ - H_+ \quad (42)$$

and where we can perturbatively expand:



Figure 1: Subdivision gadget. The  $k$ -local interaction on the left is simulated by the two  $\lceil \frac{k}{2} \rceil + 1$ -local interactions on the right by introducing a mediator qudit,  $w$ . The interactions are given by  $M_1 = P_A \otimes P_B + P_A^\dagger \otimes P_B^\dagger$ ,  $M_2 = P_A \otimes X_w + P_A^\dagger \otimes X_w^\dagger$ , and  $M_3 = P_B \otimes X_w^\dagger + P_B^\dagger \otimes X_w$ .

$$(I_+ - V_{++}G_+)^{-1} = I_+ + V_{++}G_+ + V_{++}G_+V_{++}G_+ + \dots \quad (43)$$

The general case of the theorem below was proved in [26]. Here we state the version from [30] where  $H$  has a degenerate ground space of energy zero, and the spectral gap above the ground space is  $\Delta$ .

**Theorem 3.9** ([26]). *Let  $\|V\| \leq \frac{\Delta}{2}$  where  $\Delta$  is the spectral gap of  $H$  and  $\lambda(H) = 0$ . Let  $\tilde{H}|_{\frac{\Delta}{2}}$  be the restriction of  $\tilde{H} = H + V$  to the space of eigenstates with values less than  $\frac{\Delta}{2}$ . Let there be an effective Hamiltonian  $H_{\text{eff}}$  with  $\text{Spec}(H_{\text{eff}}) \subseteq [a, b]$ . If the self-energy  $\Sigma_-(z)$  for all  $z \in [a - \epsilon, b + \epsilon]$  where  $a < b < \frac{\Delta}{2} - \epsilon$  for some  $\epsilon > 0$  has the property that:*

$$\|\Sigma_-(z) - H_{\text{eff}}\| \leq \epsilon \quad (44)$$

then each eigenvalue  $\tilde{\lambda}_j$  of  $\tilde{H}|_{\frac{\Delta}{2}}$  is  $\epsilon$ -close to the  $j$ th eigenvalue of  $H_{\text{eff}}$ . In particular:

$$|\lambda(H_{\text{eff}}) - \lambda(\tilde{H})| \leq \epsilon \quad (45)$$

All the perturbation gadgets introduced below are qudit gadgets which generalise qubit gadgets from [30]. In our analysis of the perturbation gadgets we assume without loss of generality that every interaction is a Pauli-rank 2 interaction of the form  $P_a + P_a^\dagger$ .

#### Qudit subdivision gadget

The subdivision gadget is used to break down a  $k$ -local interaction into interactions which are at most  $\lceil \frac{k}{2} \rceil + 1$ -local.

We want to generate the Hamiltonian:

$$H_{\text{target}} = H_{\text{else}} + (P_A \otimes P_B + P_A^\dagger \otimes P_B^\dagger) \quad (46)$$

Let  $\tilde{H} = H + V$  where:

$$H = \Delta \Pi_+ \quad (47)$$

$$V = \sqrt{\frac{\Delta}{2}} \left( -P_A \otimes X_w - P_A^\dagger \otimes X_w^\dagger + P_B \otimes X_w^\dagger + P_B^\dagger \otimes X_w \right) + H'_{\text{else}} \quad (48)$$

where  $\Pi_+ = |1\rangle\langle 1|_w + |2\rangle\langle 2|_w + \dots + |p-1\rangle\langle p-1|_w$  and  $H'_{\text{else}} = H_{\text{else}} + 2\mathbb{I}$ . The degenerate ground space of  $H$  has the mediator qubit  $w$  in the state  $|0\rangle\langle 0|$  so  $\Pi_- = |0\rangle\langle 0|_w$ . This gives:

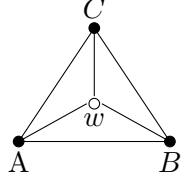


Figure 2: 3-2 gadget: The three body interaction between  $A$ ,  $B$  and  $C$   $\left(P_A \otimes P_B \otimes P_C + P_A^\dagger \otimes P_B^\dagger \otimes P_C^\dagger\right)$  is simulated by the interaction pattern shown in the figure.

$$V_{--} = H'_{\text{else}} \otimes |0\rangle\langle 0|_w \quad (49)$$

and:

$$V_{-+} = \sqrt{\frac{\Delta}{2}} \left( -P_A \otimes |0\rangle\langle p-1|_w - P_A^\dagger \otimes |0\rangle\langle 1|_w + P_B \otimes |0\rangle\langle 1|_w + P_B^\dagger \otimes |0\rangle\langle p-1|_w \right) \quad (50)$$

Therefore:

$$V_{-+} G_+ V_{+-} = -\frac{\Delta}{z - \Delta} \left( P_A \otimes P_B + P_A^\dagger \otimes P_B^\dagger - 2\mathbb{I} \right) \otimes |0\rangle\langle 0|_w \quad (51)$$

The self energy is then given by:

$$\Sigma_-(z) = \left( H'_{\text{else}} - \frac{\Delta}{z - \Delta} \left( P_A \otimes P_B + P_A^\dagger \otimes P_B^\dagger - 2\mathbb{I} \right) \right) \otimes |0\rangle\langle 0|_w + O\left(\frac{\|V\|^3}{(z - \Delta)^2}\right) \quad (52)$$

Expand the self-energy about  $z = 0$  and let  $H_{\text{eff}} = H_{\text{target}} \otimes |0\rangle\langle 0|_w$ :

$$\|\Sigma_-(z) - H_{\text{eff}}\| = O\left(\frac{|z|r^2}{\Delta}\right) + O\left(\frac{\|V\|^2}{\Delta^2}\right) + O\left(\frac{|z|\|V\|^3}{\Delta^3}\right) \quad (53)$$

where  $r = \max(\|P_A\|, \|P_B\|)$ .

Following the same analysis as in [30], if we choose:

$$\Delta \geq \frac{(\|H_{\text{else}}\| + \sqrt{2}r)^6}{\epsilon^2} \quad (54)$$

then:

$$\|\Sigma_-(z) - H_{\text{eff}}\| = O(\epsilon) \quad (55)$$

so the  $j$ th eigenvalue of  $\tilde{H}$  is  $\epsilon$ -close to the  $j$ th eigenvalue of  $H_{\text{eff}}$ .

### Qudit 3-2 gadget

The Hamiltonian we want to generate is:

$$H_{\text{target}} = H_{\text{else}} + P_A \otimes P_B \otimes P_C + P_A^\dagger \otimes P_B^\dagger \otimes P_C^\dagger \quad (56)$$

Let  $\tilde{H} = H + V$  where:

$$H = \Delta \Pi_+ \quad (57)$$

$$\begin{aligned} V = H_{\text{else}} + V_{\text{extra}} - \Delta^{\frac{2}{3}} & \left( P_C \otimes |p-1\rangle \langle 1|_w + P_C^\dagger |1\rangle \langle p-1|_w \right) \\ & + \frac{\Delta^{\frac{2}{3}}}{\sqrt{2}} \left( (-P_A + P_B) \otimes X_w + (-P_A^\dagger + P_B^\dagger) \otimes X_w^\dagger \right) \end{aligned} \quad (58)$$

where  $\Delta \Pi_+ = |1\rangle \langle 1|_w + \dots + |p-1\rangle \langle p-1|_w$ , and the correction term  $V_{\text{extra}}$  is given by:

$$\begin{aligned} V_{\text{extra}} = \Delta^{\frac{1}{3}} & \left( P_A \otimes P_B^\dagger + P_A^\dagger \otimes P_B \right) + \left( P_A^2 \otimes P_C + (P_A^\dagger)^2 \otimes P_C^\dagger + P_B^2 \otimes P_C + (P_B^\dagger)^2 \otimes P_C^\dagger \right) \\ & + \frac{1}{\sqrt{2}} \left[ (P_A + P_B)^2 \left( P_A^\dagger + P_B^\dagger \right) + \left( P_A^\dagger + P_B^\dagger \right)^2 (P_A + P_B) \right] \end{aligned} \quad (59)$$

This gives:

$$V_{--} = (H_{\text{else}} + V_{\text{extra}}) \otimes |0\rangle \langle 0|_w \quad (60)$$

$$V_{-+} = \frac{\Delta^{\frac{2}{3}}}{\sqrt{2}} \left[ (-P_A + P_B) \otimes |0\rangle \langle p-1|_w + (-P_A^\dagger + P_B^\dagger) \otimes |0\rangle \langle 1|_w \right] \quad (61)$$

$$\begin{aligned} V_{++} = -\Delta^{\frac{2}{3}} & \left( P_C \otimes |p-1\rangle \langle 1|_w + P_C^\dagger \otimes |1\rangle \langle p-1|_w \right) \\ & + \frac{\Delta^{\frac{2}{3}}}{\sqrt{2}} \left[ (-P_A + P_B) \otimes Q_w + (-P_A^\dagger + P_B^\dagger) \otimes R_w \right] \\ & + (H_{\text{else}} + V_{\text{extra}}) \otimes \Pi_+ \end{aligned} \quad (62)$$

where  $Q = |2\rangle \langle 2| + \dots + |p-1\rangle \langle p-1|$  and  $R = |1\rangle \langle 1| + \dots + |p-2\rangle \langle p-2|$ .

Therefore:

$$\begin{aligned} \Sigma_-(z) = (H_{\text{else}} + V_{\text{extra}}) \otimes |0\rangle \langle 0|_w & + \frac{\Delta^{\frac{4}{3}}}{z - \Delta} \left( -P_A \otimes P_B^\dagger - P_A^\dagger \otimes P_B \right) \otimes |0\rangle \langle 0|_w \\ & + \frac{\Delta^2}{2(z - \Delta)^2} \left( P_A^2 \otimes P_C + (P_A^\dagger)^2 \otimes P_C^\dagger + P_B^2 \otimes P_C + (P_B^\dagger)^2 \otimes P_C^\dagger \right) \otimes |0\rangle \langle 0|_w \\ & - \frac{\Delta^2}{(z - \Delta)^2} \left( -P_A \otimes P_B \otimes P_C - P_A^\dagger \otimes P_B^\dagger \otimes P_C^\dagger \right) \otimes |0\rangle \langle 0|_w + O\left(\frac{\|V\|^4}{(z - \Delta)^3}\right) \end{aligned} \quad (63)$$

Expanding  $\Sigma_-(z)$  about  $z = 0$ , and setting  $H_{\text{eff}} = H_{\text{target}} \otimes |0\rangle \langle 0|_w$  gives:

$$\|\Sigma_-(z) - H_{\text{eff}}\| = O(\Delta^{-\frac{1}{3}}) + O(|z|\Delta^{-\frac{2}{3}}) + O\left(\frac{\|V\|^4}{\Delta^3}\right) + O\left(\frac{|z|\|V\|^4}{\Delta^4}\right) \quad (64)$$

For sufficiently large  $\Delta$  we can make  $\Sigma_-(z)$  arbitrarily close to  $H_{\text{eff}}$  for the required range of  $|z|$ .

***Qudit crossing gadget***

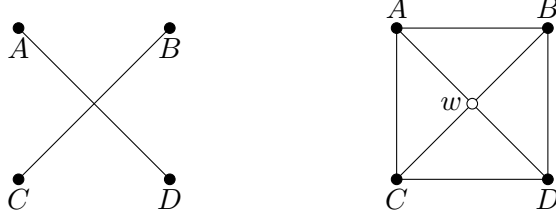


Figure 3: Crossing gadget. The interaction pattern on the left is simulated by the interaction pattern on the right.

We want to generate the Hamiltonian:

$$H_{\text{target}} = H_{\text{else}} + \alpha_{ad} (P_A \otimes P_D + P_A^\dagger \otimes P_D^\dagger) + \alpha_{bc} (P_B \otimes P_C + P_B^\dagger \otimes P_C^\dagger) \quad (65)$$

Set  $\tilde{H} = H + V$  where:

$$H = \Delta \Pi_+ \quad (66)$$

$$V = \sqrt{\frac{\Delta}{2}} [-\alpha_{ad}(P_A \otimes X_w + P_A^\dagger \otimes X_w^\dagger) - \alpha_{bc}(P_B \otimes X_w + P_B^\dagger \otimes X_w^\dagger) + (P_C \otimes X_w^\dagger + P_C^\dagger \otimes X_w) + (P_D \otimes X_w^\dagger + P_D^\dagger \otimes X_w)] + H'_{\text{else}} \quad (67)$$

where:

$$\begin{aligned} H'_{\text{else}} = H_{\text{else}} + & [\alpha_{ad}\alpha_{bc}(P_A \otimes P_B^\dagger + P_A^\dagger \otimes P_B) - \alpha_{ad}(P_A \otimes P_C^\dagger + P_A^\dagger \otimes P_C) \\ & - \alpha_{bc}(P_B \otimes P_D^\dagger + P_B^\dagger \otimes P_D) + (P_C \otimes P_D^\dagger + P_C^\dagger \otimes P_D) \\ & + \mathbb{I}(\alpha_{ad}^2 + \alpha_{bc}^2 + 2)] \end{aligned} \quad (68)$$

Then:

$$V_{--} = H'_{\text{else}} \otimes |0\rangle \langle 0|_w \quad (69)$$

$$\begin{aligned} V_{-+} = \sqrt{\frac{\Delta}{2}} & [-\alpha_{ad}(P_A \otimes |0\rangle \langle p-1|_w + P_A^\dagger |0\rangle \langle 1|_w) - \alpha_{bc}(P_B \otimes |0\rangle \langle p-1|_w + P_B^\dagger |0\rangle \langle 1|_w) \\ & + (P_C \otimes |0\rangle \langle 1|_w + P_C^\dagger |0\rangle \langle p-1|_w) + (P_D \otimes |0\rangle \langle 1|_w + P_D^\dagger |0\rangle \langle p-1|_w)] \end{aligned} \quad (70)$$

Therefore:

$$\begin{aligned} \Sigma_-(z) = & \left( H'_{\text{else}} + \frac{\Delta}{z - \Delta} \left[ -\alpha_{ad} (P_A \otimes P_D + P_A^\dagger \otimes P_D^\dagger) - \alpha_{bc} (P_B \otimes P_C + P_B^\dagger \otimes P_C^\dagger) \right] \right) \otimes |0\rangle \langle 0|_w \\ & + \frac{\Delta}{z - \Delta} [H'_{\text{else}} - H_{\text{else}}] \otimes |0\rangle \langle 0|_w + O\left(\frac{\|V\|^3}{(z - \Delta)^2}\right) \end{aligned} \quad (71)$$



Figure 4: Fork gadget. The interaction pattern on the left is simulated by the interaction pattern on the right.

Expanding  $\Sigma_-(z)$  about  $z = 0$  and setting  $H_{\text{eff}} = H_{\text{target}} \otimes |0\rangle\langle 0|_w$  gives:

$$\|\Sigma_-(z) - H_{\text{eff}}\| = O\left(\frac{|z|r^2}{\Delta}\right) + O\left(\frac{\|V\|^2}{\Delta^2}\right) + O\left(\frac{|z|\|V\|^3}{\Delta^3}\right) \quad (72)$$

where  $r = \max(P_A, P_B, P_C, P_D)$ .

For sufficiently large  $\Delta$  we can make  $\Sigma_-(z)$  arbitrarily close to  $H_{\text{eff}}$  for the required range of  $|z|$ .

### Qudit fork gadget

We want to generate the Hamiltonian:

$$H_{\text{target}} = H_{\text{else}} + \alpha_{ab} (P_A \otimes P_B + P_A^\dagger \otimes P_B^\dagger) + \alpha_{ac} (P_A \otimes P_C + P_A^\dagger \otimes P_C^\dagger) \quad (73)$$

Let  $\tilde{H} = H + V$  where:

$$H = \Delta \Pi_+ \quad (74)$$

$$\begin{aligned} V = H'_{\text{else}} + \sqrt{\frac{\Delta}{2}} &(-(P_A \otimes X_w + P_A^\dagger \otimes X_w^\dagger) + \alpha_{ab}(P_B \otimes X_w^\dagger + P_B^\dagger \otimes X_w) \\ &+ \alpha_{ac}(P_C \otimes X_w^\dagger + P_C^\dagger \otimes X_w)) \end{aligned} \quad (75)$$

where:

$$H'_{\text{else}} = H_{\text{else}} + \alpha_{ab}\alpha_{ac} (P_B \otimes P_C^\dagger + P_B^\dagger \otimes P_C) + \mathbb{I}(1 + \alpha_{ab}^2 + \alpha_{ac}^2) \quad (76)$$

Then:

$$V_{--} = H'_{\text{else}} \otimes |0\rangle\langle 0|_w \quad (77)$$

$$\begin{aligned} V_{-+} = \sqrt{\frac{\Delta}{2}} &[-(P_A \otimes |0\rangle\langle p-1|_w + P_A^\dagger \otimes |0\rangle\langle 1|_w) + \alpha_{ab}(P_B \otimes |0\rangle\langle 1|_w + P_B^\dagger \otimes |0\rangle\langle p-1|_w) \\ &+ \alpha_{ac}(P_C \otimes |0\rangle\langle 1|_w + P_C^\dagger \otimes |0\rangle\langle p-1|_w)] \end{aligned} \quad (78)$$

Therefore:

$$\Sigma_-(z) = H'_{\text{else}} \otimes |0\rangle\langle 0|_w - \frac{\Delta}{z - \Delta} H_{\text{target}} \otimes |0\rangle\langle 0| + \frac{\Delta}{z - \Delta} (H'_{\text{else}} - H_{\text{else}}) \otimes |0\rangle\langle 0| + O\left(\frac{\|V\|^3}{(z - \Delta)^2}\right) \quad (79)$$



Figure 5: Triangle gadget. The interaction pattern on the left is simulated by the interaction pattern on the right by first applying the subdivision gadget to edges  $AB$  and  $AC$ , and then applying the fork gadget to qudit  $A$ .

Expanding  $\Sigma_-(z)$  about  $z = 0$  and setting  $H_{\text{eff}} = H_{\text{target}} \otimes |0\rangle\langle 0|_w$  gives:

$$\|\Sigma_-(z) - H_{\text{eff}}\| = O\left(\frac{|z|r^2}{\Delta}\right) + O\left(\frac{\|V\|^2}{\Delta^2}\right) + O\left(\frac{|z|\|V\|^3}{\Delta^3}\right) \quad (80)$$

where  $r = \max(P_A, P_B, P_C)$ .

For sufficiently large  $\Delta$  we can make  $\Sigma_-(z)$  arbitrarily close to  $H_{\text{eff}}$  for the required range of  $|z|$ .

#### Qudit triangle gadget

The qudit triangle gadget is formed by first applying the qudit subdivision gadget, then the qudit fork gadget, in the same way as it is formed for qubits in [30].

In [30] it is demonstrated that the qubit perturbation gadgets can be used at many places in an interaction graph in parallel, and that they do not interact with each other. The same arguments follows for the qudit perturbation gadgets introduced here.

#### 3.5.4 Perturbative simulations

In [6] a number of results were shown that demonstrate perturbative reductions can generate simulations.

Let  $H = \Delta H_0$ , where  $H_0$  is block-diagonal with respect to the split  $\mathcal{H} = \mathcal{H}_- \oplus \mathcal{H}_+$ ,  $(H_0)_{--} = 0$ ,  $\lambda_{\min}((H_0)_{++}) \geq 1$ .

**Lemma 3.10** (First order simulation [6]). *Let  $V = H_1$  be a perturbation acting on the same space as  $H_0$ . Suppose there exists an isometry  $W$  such that  $\text{Im}(W) = \mathcal{H}_-$  and:*

$$\|WH_{\text{target}}W^\dagger - (H_1)_{--}\| \leq \frac{\epsilon}{2} \quad (81)$$

*Then  $\tilde{H} = H + V$  ( $\frac{\Delta}{2}, \eta, \epsilon$ ) simulates  $H_{\text{target}}$ , provided that the bound  $\Delta \geq O(\frac{\|H_1\|^2}{\epsilon} + \frac{\|H_1\|}{\eta})$  holds.*

**Lemma 3.11** (Second order simulation [6]). *Let  $V = H_1 + \Delta^{\frac{1}{2}}H_2$  be a perturbation acting on the same space as  $H_0$  such that  $\max(\|H_1\|, \|H_2\|) \leq \Lambda$ ;*

$H_1$  is block diagonal with respect to the split  $\mathcal{H} = \mathcal{H}_- \oplus \mathcal{H}_+$  and  $(H_2)_{--} = 0$ . Suppose there exists an isometry  $W$  such that  $\text{Im}(W) = \mathcal{H}_-$  and:

$$\|WH_{\text{target}}W^\dagger - (H_1)_{--} + (H_2)_{-+}H_0^{-1}(H_2)_{+-}\| \leq \frac{\epsilon}{2} \quad (82)$$

Then  $\tilde{H} = H + V \left(\frac{\Delta}{2}, \eta, \epsilon\right)$  simulates  $H_{\text{target}}$ , provided that  $\Delta \geq O\left(\frac{\Lambda^6}{\epsilon^2} + \frac{\Lambda^2}{\eta^2}\right)$ .

**Lemma 3.12** (Third order simulation [6]). *Let  $V = H_1 + \Delta^{\frac{1}{3}}H'_1 + \Delta^{\frac{2}{3}}H_2$  be a perturbation acting on the same space as  $H_0$  such that  $\max(\|H_1\|, \|H'_1\|, \|H_2\|) \leq \Lambda$ ;  $H_1$  and  $H'_1$  are block diagonal with respect to the split  $\mathcal{H} = \mathcal{H}_- \oplus \mathcal{H}_+$  and  $(H_2)_{--} = 0$ . Suppose there exists an isometry  $W$  such that  $\text{Im}(W) = \mathcal{H}_-$  and:*

$$\|WH_{\text{target}}W^\dagger - (H_1)_{--} + (H_2)_{-+}H_0^{-1}(H_2)_{++}H_0^{-1}(H_2)_{+-}\| \leq \frac{\epsilon}{2} \quad (83)$$

and also that:

$$(H'_1)_{--} = (H_2)_{-+}H_0^{-1}(H_2)_{+-} \quad (84)$$

Then  $\tilde{H} = H + V \left(\frac{\Delta}{2}, \eta, \epsilon\right)$  simulates  $H_{\text{target}}$ , provided that  $\Delta \geq O\left(\frac{\Lambda^{12}}{\epsilon^3} + \frac{\Lambda^3}{\eta^3}\right)$ .

In [9] it was shown that these results still hold if we restrict  $W$  to be a local isometry.

All of the perturbative gadgets introduced in the preceding section meet the requirements to be simulations for appropriate choices of  $\Delta$ .<sup>15</sup> The isometry in each case is defined by  $W|\psi\rangle_A = |\psi\rangle_A|0\rangle_c$ .

## 4 Holographic quantum error correcting codes and complete bulk-boundary dualities

### 4.1 Notation

Let  $(W, S)$  be a Coxeter system with Coxeter polytope  $P \subseteq \mathbb{H}^3$ .  $F_a$  denotes the face of  $P$  which corresponds to the generator  $s_a \in S$ .  $E_{ab}$  denotes the edge of  $P$  between faces  $F_a$  and  $F_b$ .

$P^{(w)}$  denotes the polyhedral cell in the tessellation of  $\mathbb{H}^3$  by  $P$  which corresponds to element  $w$  of the Coxeter group. Similarly  $F_a^{(w)}$  and  $E_{ab}^{(w)}$  refer to faces / edges of  $P^{(w)}$ .  $F_a^A$  and  $E_{ab}^A$  refer to specific faces / edges in the tessellation of  $\mathbb{H}^3$  which are shared by the polyhedral cells associated to the sets of elements  $A \subseteq W$ .

A bulk qudit which is associated to the polyhedral cell  $P^{(w)}$  will be labelled by  $q^{(w)}$ . A boundary qudit which is associated to the uncontracted tensor index through the face  $F_a^{(w)}$  will be labelled by  $q_a^{(w)}$ .

---

<sup>15</sup>The 3-2 qudit perturbation gadget is a third order simulation, the other gadgets are all second order simulations.

## 4.2 General construction

In this section we will demonstrate the general procedure for constructing a HQECC using Coxeter groups and (pseudo-)perfect stabilizer tensors with particular properties. In particular in Section 4.2.5 we prove our main result - that we can construct a complete holographic duality between 3D hyperbolic space and its 2D boundary. In Sections 4.3 and 4.4 we will provide two examples of sets of Coxeter groups and tensors which have the required properties.

### 4.2.1 Holographic quantum error correcting codes

The procedure we use to construct the tensor network is based on that in [31], where perfect tensors are embedded in tessellations of  $\mathbb{H}^2$ . We take a Coxeter system  $(W, S)$  with Coxeter polytope,  $P \subseteq \mathbb{H}^3$  where  $|S| = t - 1$ , so  $P$  has  $t - 1$  faces. Take the tessellation of  $\mathbb{H}^3$  by  $P$ , and embed a (pseudo-)perfect tensor,  $T$ , with  $t$  legs in each polyhedral cell.  $t - 1$  legs of each (pseudo-)perfect tensor are contracted with legs of neighbouring tensors at shared faces of the polyhedra, and a logical, or input, qudit for the tensor network is associated with the uncontracted tensor leg in each polyhedral cell. Cut off the tessellation at some radius  $R$ , and the uncontracted tensor legs on the boundary are the physical qudits of the tensor network.

A HQECC is defined as a tensor network composed of (pseudo)-perfect tensors which gives rise to an isometric map from bulk legs to boundary legs [31]. As the tensor network we have described is composed of (pseudo-)perfect tensors, it will be an isometric map from bulk legs to boundary legs provided that the number of output legs from every tensor is greater than or equal to the number of input legs, where the input legs are the legs coming from the previous layer of the tessellation plus the logical leg.

We are working in negatively curved geometry, so on average the number of output legs will be greater than the number of input legs, but this doesn't guarantee that every tensor will have more output legs than input legs. For example, consider the triangulation of  $\mathbb{H}^2$  with Schläfli symbol  $\{3, 8\}$  (Fig. 6). This is the tiling which corresponds to the Coxeter diagram shown in Fig. 7.

It can be seen that there are triangular cells in the tessellation which share edges with two triangles from the previous layer, and only one in the subsequent layer. If we put a four-index perfect tensor in each cell of this tessellation, then there would be some tensors with three input legs, and only one output leg. These tensors would not be isometries, so it is not obvious that the overall tensor network would be an isometry from input legs to output legs, and therefore that the tensor network would be a HQECC. In order to ensure that the tensor network is a HQECC we derive a condition to enforce that every tensor in our tensor networks has at least as many output indices as input indices. This is a sufficient condition for the tensor network

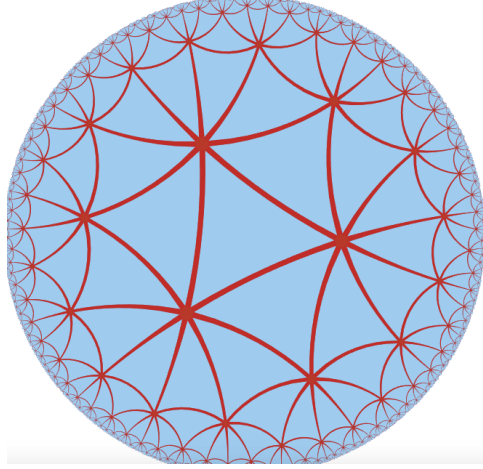


Figure 6: The triangulation of  $\mathbb{H}^2$  with Schläfli symbol  $\{3,8\}$ . There are triangular cells in the tessellation which share edges with two triangles from the previous layer, and only one in the subsequent layer. Figure produced via the software [42].

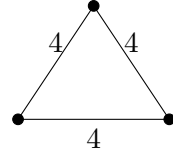


Figure 7: The Coxeter diagram for the triangulation of  $\mathbb{H}^2$  with Schläfli symbol  $\{3,8\}$

to be a HQECC, but it may not be necessary.

**Theorem 4.1.** *Consider a tensor network constructed as above, defined by Coxeter system  $(W, S)$  and perfect tensor  $T$  with  $t$  indices. Define  $\mathcal{F} = \{J \subseteq S \mid W_J \text{ is finite}\}$ . The tensor network will be a HQECC, if  $\forall J \in \mathcal{F} : |J| \leq \lfloor \frac{t-2}{2} \rfloor$ .*

*Proof.* If we order the tensors into layers labelled by the value of the length function  $l_S(w)$  at  $P^{(w)}$ , and include the uncontracted tensor leg in each polyhedral cell as an input leg, then the number of input legs for a tensor embedded in  $P^{(w)}$  is  $\mathcal{D}_R(w) + 1$ . By Lemma 3.7,  $\mathcal{D}_R(w) \in \mathcal{F}$ . Therefore the maximum number of input legs to any tensor in the tensor network is  $\max(|J| \mid J \in \mathcal{F}) + 1$ . We therefore require  $\max(|J| \mid J \in \mathcal{F}) + 1 \leq \lfloor \frac{t}{2} \rfloor$ .  $\square$

Theorem 4.1 gives a sufficient condition for every tensor in the tensor network to have at least as many output indices as input indices. It is not clear whether this condition is also necessary.

The requirements of Theorem 4.1 dictate that we will not be able to use qubit stabilizer tensors to construct HQECC in dimensions greater than two. To see this recall that Lemma 3.6 stated that  $\{s_i \mid i \in I\}$  generates a finite Coxeter group if and only if  $f = \cup_{i \in I} F_i$  is a codimension  $|I|$  face of  $P$ . In dimension  $d$  there will exist codimension  $d$  faces, so  $\max(|J| \mid J \in \mathcal{F}) \geq d$ . We therefore require that  $\lfloor \frac{t}{2} \rfloor \geq d + 1$ . For  $d \geq 3$  this enforces  $t \geq 8$ , and there are no qubit perfect tensors with  $t > 6$  [14, 33, 25].

HQECC which are constructed in this way inherit all the properties of the 2-dimensional HQECC constructed in [31].

#### 4.2.2 Surface of the HQECC

Define the boundary of the HQECC as the faces in the tessellation which correspond to the uncontracted tensor legs. More precisely:

**Definition 11.** *The boundary,  $M$ , of a HQECC of radius  $R$  is given by:*

$$M = \bigcup_{F_a^{(w)} \in \mathcal{M}} F_a^{(w)} \quad (85)$$

where  $\mathcal{M} = \{F_a^{(w)} \mid l_S(w) = R, s_a \in \mathcal{A}_R(w)\}$ .

The boundary of hyperbolic  $n$ -space is an  $n - 1$  dimensional sphere. For our HQECC we are cutting off the tessellation of  $\mathbb{H}^3$  at some finite radius  $R$ , but it is still possible to demonstrate that the boundary of the HQECC is homeomorphic to a 2-sphere.

In order to reason about the boundary we first need two lemmas about edges in the tessellation of  $\mathbb{H}^3$  by  $P$ :

**Lemma 4.2.** *Consider an edge,  $E_{ab}^A$ , in the tessellation of  $\mathbb{H}^3$  by a Coxeter polytope,  $P$ . If  $l_S(w_1) = l_S(w_2) = L$  for distinct  $w_1, w_2 \in A$ , then  $\mathcal{D}_R(w_1)$  and  $\mathcal{D}_R(w_2)$  contain at least one of  $s_a$  or  $s_b$ .*

*Proof.* Recall that an edge  $E_{ab}$  corresponds to the finite Coxeter subgroup generated by  $s_a$  and  $s_b$ :  $\langle s_a, s_b \rangle = \{\langle s_a, s_b \rangle^x \mid x \in [0, m_{ab}]\}$ , where  $\langle s_a, s_b \rangle^x$  denotes a string of alternating  $s_a$  and  $s_b$  of length  $x$ .  $A$  is set of Coxeter group elements corresponding to the polyhedra that meet at the common edge  $E_{ab}^A$ , so  $A = \{ws \mid s \in \langle s_a, s_b \rangle\}$  for any fixed element  $w \in A$ . Therefore, we have that  $w_2 =_w w_1 \langle s_a, s_b \rangle^x$  for some  $x \in [1, m_{ab}]$ ; we take  $x$  to be the minimum such value. Since  $l_S(w_1 \langle s_a, s_b \rangle^x) = l_S(w_2) + x > l_S(w_2)$ , the deletion condition (Definition 7) implies that there are two generators in the word  $w_1 \langle s_a, s_b \rangle^x$  which we can delete to get a shorter word for  $w_2$ .

By minimality of  $x$ , they cannot both be deleted from the  $\langle s_a, s_b \rangle^x$  part of this word. If they were both deleted from the  $w_1$  part, so that  $w_2 =_w s_1 \dots \hat{s}_i \dots \hat{s}_j \dots s_L \langle s_a s_b \rangle^x$ , we would have  $w_1 =_w w_2 (\langle s_a, s_b \rangle^x)^{-1} = w_2 \langle s_b, s_a \rangle^x =_w s_1 \dots \hat{s}_i \dots \hat{s}_j \dots s_L$  which has length  $L - 2$ , contradicting

$l_S(w_1) = L$ . Therefore, one generator must be deleted from the  $w_1$  part, the other from  $\langle s_a, s_b \rangle^x$ . Thus  $w_2 =_w s_1 \dots \hat{s}_i \dots s_r \langle s_a, s_b \rangle^{x-1}$ .

This word for  $w_2$  has length  $L + x - 2$ . By the deletion condition, we must be able to delete a further  $x - 2$  generators to reach a reduced word for  $w_2$ . But  $\langle s_a, s_b \rangle^{x-1}$  contains  $x - 1$  generators, so at least one of these must remain. Thus either  $w_2 =_w us_a$  or  $w_2 =_W us_b$  for some  $u \in A$  of length  $l_S(u) = L - 1$ . Hence at least one of  $s_a$  or  $s_b$  is in  $\mathcal{D}_R(w_2)$ .

The  $w_1$  case follows by an analogous argument.  $\square$

**Lemma 4.3.** *Consider an edge,  $E_{ab}^A$ , in the tessellation of  $\mathbb{H}^3$  by a Coxeter polytope,  $P$ . The set of elements  $A$  associated with the polyhedral cells that share the edge  $E_{ab}^A$  has the following properties:*

- (i) *There is a unique minimum length element  $w_{\min} \in A$  which has length,  $l_S(w_{\min}) = r_{\min}$ .*
- (ii) *For  $0 \leq x < m_{ab}$ ,  $l_S(w_{\min} \langle s_a, s_b \rangle^{x+1}) = l_S(w_{\min} \langle s_a, s_b \rangle^x) + 1$ .*
- (iii) *For  $m_{ab} \leq x < 2m_{ab}$ ,  $l_S(w_{\min} \langle s_a, s_b \rangle^{x+1}) = l_S(w_{\min} \langle s_a, s_b \rangle^x) - 1$ .*
- (iv) *There is a unique maximum length element  $w_{\max} \in A$  which has length  $l_S(w_{\max}) = r_{\min} + m_{ab}$ .*
- (v) *For  $r_{\min} < i < r_{\min} + m_{ab}$  there are exactly two elements  $w_i, w'_i \in A$  which satisfy  $l_S(w_i) = l_S(w'_i) = i$ .*

where  $\langle s_a, s_b \rangle^x$  denotes a string of alternating  $s_a$  and  $s_b$  of length  $x$  (i.e.  $\langle s_a, s_b \rangle^3 = s_a s_b s_a$ ).

*Proof of Lemma 4.3.* i. Assume there are two minimum length elements in  $A$ ,  $w_{\min}$  and  $w'_{\min}$  such that  $l_S(w_{\min}) = l_S(w'_{\min}) = r_{\min}$ . By Lemma 4.2 either  $s_a$  or  $s_b$  is in the descent set of  $w_{\min}$  and  $w'_{\min}$ . This implies that there is at least one element in  $A$  with length  $r_{\min} - 1$ , contradicting our assumption that  $w_{\min}$  and  $w'_{\min}$  are the minimum length elements in  $A$ . Therefore there is a unique minimum length element  $w_{\min} \in A$ .

ii. Assume there is some  $x < m_{ab}$  such that  $l_S(w_{\min} \langle s_a, s_b \rangle^{x+1}) = l_S(w_{\min} \langle s_a, s_b \rangle^x) - 1 = L$ . If we let  $u = w_{\min} \langle s_a, s_b \rangle^{x+1}$  and assume (wlog) that  $x$  is even, it follows that  $s_a \in \mathcal{A}_R(u)$ . Note that  $l_S(w_{\min}) = r_{\min} < L$ ,  $l_S(w_{\min} \langle s_a, s_b \rangle^x) = L + 1$  and  $l_S(w_{\min} \langle s_a, s_b \rangle^{x+1}) = L$ . But each generator  $s_a$  or  $s_b$  that we multiply  $w_{\min}$  by can only change the length by  $\pm 1$ . So  $u$  is not the only element of length  $L$  in  $A$ . By Lemma 4.2 this implies that at least one of  $s_a$  or  $s_b$  must be in the descent set of  $u$ . Therefore  $s_b \in \mathcal{D}_R(u)$ .

If we let  $v = us_b$  then  $s_b \in \mathcal{A}_R(v)$ . By a similar argument,  $s_a \in \mathcal{D}_R(v)$ . If we continue this argument we find that the length of the element  $w_{\min} \langle s_a, s_b \rangle^{2x}$  is  $r_{\min}$ , which is not possible as  $w_{\min}$  is the unique element of  $A$  with length  $r_{\min}$ , and by assumption  $x < m_{ab}$  so  $\langle s_a, s_b \rangle^{2x} =$

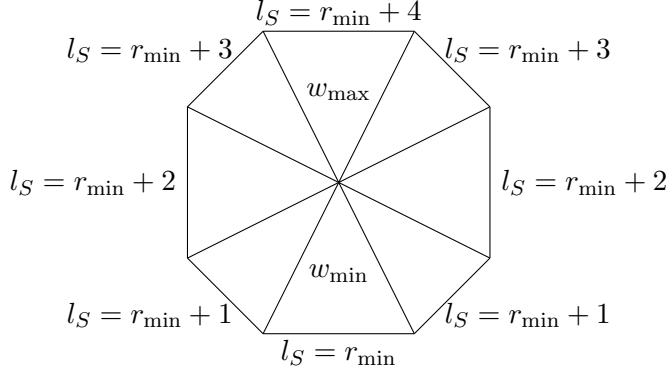


Figure 8: A cross section view of the polyhedral cells in the tessellation which meet around a common edge,  $E_{ab}$ , for  $m_{ab} = 4$ .

$(s_a s_b)^x \neq I$  by definition of  $m_{ab}$ . Therefore there is no  $x < m_{ab}$  such that  $l_S(w_{\min} \langle s_a, s_b \rangle^{x+1}) = l_S(w_{\min} \langle s_a, s_b \rangle^x) - 1 = L$ .

**iii.** From **ii** it follows that  $l_S(w_{\min} \langle s_a, s_b \rangle^{m_{ab}}) = r_{\min} + m_{ab}$ . We have that  $\langle s_a, s_b \rangle^{2m_{ab}} = (s_a s_b)^{m_{ab}} = I$ , thus  $l_S(w_{\min} \langle s_a, s_b \rangle^{2m_{ab}}) = l_S(w_{\min}) = r_{\min}$ . As each generator can only change the length of an element by  $\pm 1$ , for  $m_{ab} < x \leq 2m_{ab}$  we must have that  $l_S(w_{\min} \langle s_a, s_b \rangle^{x+1}) = l_S(w_{\min} \langle s_a, s_b \rangle^x) - 1$ .

**iv** and **v** follow at once from points **ii** and **iii**.  $\square$

An example of the set of polyhedra associated with an edge  $E_{ab}$  where  $m_{ab} = 4$  is shown in Fig. 8. Lemma 4.3 ensures that the lengths associated to the polyhedra around any edge follow the same pattern.

We can now consider the boundary of the HQECC.

**Lemma 4.4.** *The boundary  $M$  of a HQECC is a surface (a 2D manifold).*

*Proof.* Within the faces that make up the boundary  $M$  is clearly locally Euclidean. At the edges where the faces meet  $M$  will be locally Euclidean provided no more than two faces meet at an edge. By point (v) from Lemma 4.3 no more than two faces which form part of the boundary can meet at a given edge, so the boundary  $M$  is a surface.  $\square$

**Lemma 4.5.** *The boundary manifold,  $M$ , of the HQECC is closed - i.e. compact and with no boundary.*

*Proof.* Assume  $M$  has a boundary. This implies that  $\exists w \in W$  such that  $l_S(w) = R$  where  $F_a^{(w)} \in M$  and  $E_{a,b}^{(w)} \in \partial M$ .

Since  $E_{a,b}$  is an edge of  $P$  we must have that  $\{s_a, s_b\} \in \mathcal{F}$  where  $\mathcal{F} = \{J \subseteq S \mid W_J \text{ is finite}\}$ . This implies that  $\exists m_{ab} \in \mathbb{N} \setminus \{1\}$  such that  $(s_a s_b)^{m_{ab}} = (s_b s_a)^{m_{ab}} = I$ .

$E_{a,b}^{(w)} \in \partial M$  implies that  $F_b^{(w)} \notin M$ , and therefore  $s_b \in \mathcal{D}_R(w)$ . This gives  $w =_w us_b$  where  $u \in W$  and  $l_S(u) = R - 1$ . We also have that  $l_S(ws_a) = l_S(us_b s_a) = R + 1$  (because by assumption  $s_a \in \mathcal{A}_R(w)$ ).

Putting everything together we find that:

$$l_S(u) = R - 1 \quad (86)$$

$$l_S(us_b s_a) = R + 1 \quad (87)$$

$$l[u(s_b s_a)^{m_{ab}}] = l_S(u) = R - 1 \quad (88)$$

Therefore, at least one of the following must be true:

1.  $\exists x$  such that  $1 \leq x < m_{ab}$  where  $l[u(s_b s_a)^x] = R + 1$  and  $l[u(s_b s_a)^x s_b] = R$
2.  $\exists x$  such that  $1 \leq x < m_{ab}$  where  $l[u(s_b s_a)^x s_b] = R + 1$  and  $l[u(s_b s_a)^{x+1}] = R$

The second case would imply that  $l[u(s_b s_a)^x s_b] = R + 1 = l_S(us_b s_a)$  but this cannot occur as it is not possible for two elements of the Coxeter group with the same word length to be related by an odd number of generators, so the first case must occur. But, if the first case occurs then  $F_v^{(b)} \in M$  for  $v = u(s_b s_a)^x s_b$  and shares edge  $E_{ab}$  with  $F_w^{(a)}$ , so  $E_{ab}^{(w)} \notin \partial M$ .

Therefore  $M$  does not have a boundary. The boundary of every polyhedron face is included in  $M$  so  $M$  is compact, hence  $M$  is closed.  $\square$

We now prove that the boundary surface is orientable. A smooth surface is orientable if a continuously varying normal vector can be defined at every point on the surface. This normal vector defines the positive side of the surface (the side the normal vector is pointing to) and a negative side (the side the normal vector points away from). If the surface has a boundary, the normal vector defines an *orientation* on the boundary curve, with the following convention: standing on the positive side of the surface, and walking around the boundary curve in the direction of the orientation, the surface is always on our left.

**Lemma 4.6.** *The boundary surface,  $M$ , of the HQECC is orientable.*

*Proof.* A piecewise smooth manifold (such as  $M$ ) is orientable if, whenever two smooth component surfaces join along a common boundary, they induce *opposite* orientation on the common boundary.

Define the unit normal vector,  $\hat{n}$ , to a face  $F_a^{(w)} \in M$  to be the unit vector which is perpendicular to  $F_a^{(w)}$  and points away from  $P^{(w)}$  (i.e. it points into  $P^{(v)}$  where  $v = ws_A$ ).

Consider the two possible configurations that could occur when two faces meet at a common edge. If the two faces always induce opposite orientation

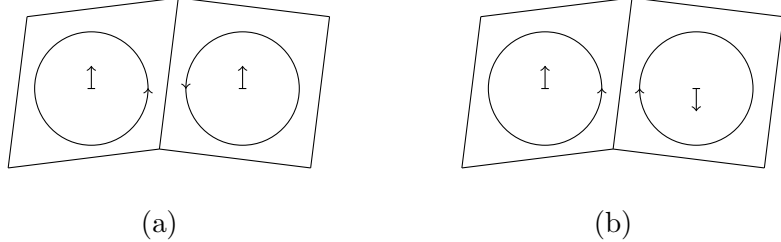


Figure 9: A cross section image of two possibilities for the orientation of faces that meet at a common edge in  $M$ . In (a) the two faces will induce opposite orientation on the common edge  $E$ , while in (b) the two faces will induce the same orientation on the common edge  $E$ .

on the common edge (as in Fig. 9 (a)) then  $M$  is orientable. If the two faces ever induce the same orientation on the common edge (as in Fig. 9 (b)) then  $M$  is not orientable.

If two faces which meet at a common edge of  $M$  are part of the same polyhedral cell of the tessellation, i.e. they are faces  $F_a^{(u)}$  and  $F_b^{(u)}$ , then it is guaranteed that the orientation of the surfaces will correspond to that shown in Fig. 9 (a) as  $\hat{n}$  is defined to point away from  $P^{(u)}$ .

If two faces which meet at a common edge of  $M$  are part of different polyhedral cells then parts (ii) and (iii) of Lemma 4.3 enforce that the orientation of the surfaces will always correspond to that shown in Fig. 9 (a).

Therefore  $M$  is orientable.  $\square$

**Lemma 4.7.** *The boundary surface,  $M$ , of the HQECC is connected.*

*Proof.* Let the boundary surface,  $M$  be a sum of connected components, where we denote the  $i^{th}$  connected component by  $M^{(i)}$ .  $M$  is closed and orientable so by the classification of surface theorem it is the sum of spheres and connected sums of tori. Both spheres and tori have well defined interiors and exteriors, so we can define the interior and exterior of each  $M^{(i)}$ .

Define the interior of  $M^{(i)}$  to be the region that  $\hat{n}^{(i)}$  points away from (i.e. the interior of  $M^{(i)}$  contains  $P^{(u)}$  for  $F_a^{(u)} \in M^{(i)}$ ,  $l_S(u) = R$ ). The exterior of  $M^{(i)}$  is then the region that  $\hat{n}^{(i)}$  points into (i.e. the exterior of  $M^{(i)}$  contains  $P^{(v)}$  for  $v = us_a$  where  $F_a^{(u)} \in M^{(i)}$ ,  $l_S(v) = R + 1$ ).

It follows from this definition that the exterior of each  $M^{(i)}$  must be unbounded. To see this, note that for an infinite Coxeter group,  $W$ , every  $w \in W$  has a non-empty  $\mathcal{A}_R(w)$ . This means that for arbitrary  $w \in W$  there exists  $s_a \in S$  such that  $l_S(ws_a) = l_S(w) + 1$ . In terms of the HQECC this implies that the number of polyhedra in the exterior of any  $M^{(i)}$  is infinite, so the exterior of  $M^{(i)}$  is unbounded.

Assume that  $M = \cup_i M^{(i)}$  is composed of more than one connected component  $M^{(i)}$ . Consider any two components  $M^{(1)}$  and  $M^{(2)}$ . There are three possible configurations:

1.  $M^{(1)}$  and  $M^{(2)}$  intersect.
2.  $M^{(2)}$  is in the interior of  $M^{(1)}$  (see Fig. 10).
3.  $M^{(2)}$  is in the exterior of  $M^{(1)}$  (see Fig. 11).

However, Case 1 would imply that  $M$  is not a surface, contradicting Lemma 4.4. Thus we only need to consider Cases 2 and 3.

The Coxeter group, and therefore the HQECC, contains a unique identity element of length  $l_S(I) = 0$ . For any  $v \in W$  such that  $l_S(v) = R$  we can write a reduced word for  $v$  as  $v =_w s_1^{(v)} s_2^{(v)} \dots s_R^{(v)}$ . Using the fact that all the generators are involutions, it follows that  $vs_R^{(v)} \dots s_2^{(v)} s_1^{(v)} =_w I$ . We started with an element of length  $R$ , and applied  $R$  generators to reach an element of length 0. Since each generator can only change the length of the previous element by  $\pm 1$  it follows that each generator must have decreased the length of the element by 1. Therefore in the HQECC there is a path through the tessellation from a polyhedra associated with an element of length  $R$  to  $P^{(I)}$  which passes through  $R$  polyhedra, all associated with elements of length less than  $R$ .

From the definition of the interior and exterior of  $M^{(i)}$  it is clear that all polyhedra which lie directly on the interior of a given  $M^{(i)}$  (i.e. those that are in the interior of  $M^{(i)}$  and touching  $M^{(i)}$ ) are associated with Coxeter group elements of length  $R$ . While all polyhedra which lie directly on the exterior of a given  $M^{(i)}$  (i.e. those that are in the exterior of  $M^{(i)}$  and touching  $M^{(i)}$ ) are associated with Coxeter group elements of length  $R + 1$ .

Therefore there must always be a path from polyhedra directly on the interior of a  $M^{(i)}$  to  $P^{(I)}$  which doesn't cross  $M^{(i)}$ . In Fig. 10 and Fig. 11 it is clear that there is no location for  $P^{(I)}$  which meets this condition. Therefore  $M$  cannot be made up of more than one connected component.  $\square$

**Lemma 4.8.** *The surface  $M$  is homeomorphic to the 2-sphere.*

*Proof.* By the classification theorem of closed surfaces, every connected closed surface is homeomorphic to either the sphere, a connected sum of tori, or a connected sum of real projective planes. Since  $M$  is orientable, it is either homeomorphic to a sphere, or a connected sum of tori.

Consider a loop  $\mathcal{C}$ , on the surface  $M$ . This loop is across faces which make up  $M$ , which are all associated to polyhedral cells of the tessellation corresponding to Coxeter group elements of length  $R$ . Since  $M$  is closed (Lemma 4.5), it cannot pinch down to a single point anywhere. Thus for any polyhedral vertex in  $M$ ,  $M$  must contain at least two faces that meet

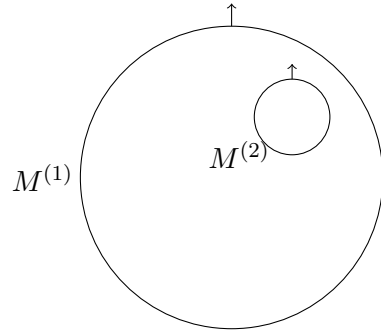


Figure 10: The configuration of  $M^{(1)}$  and  $M^{(2)}$  when  $M^{(2)}$  is in the interior of  $M^{(1)}$ . The arrows are the  $\hat{n}^{(i)}$  which point into the exterior of each surface. The polyhedra which lie directly on the interior of a given  $M^{(i)}$  are associated with Coxeter group elements of length  $R$ , while the polyhedra which lie directly on the exterior of a given  $M^{(i)}$  are associated with Coxeter group elements of length  $R + 1$ . Although we have drawn  $M^{(1)}$  and  $M^{(2)}$  as circles we are not assuming they are spherical, they could be tori, all we are assuming is that they have a well defined interior and exterior.

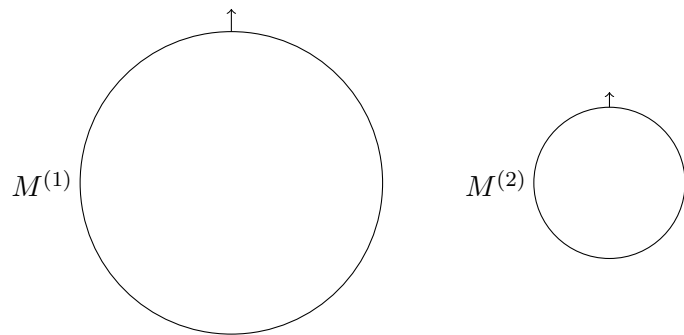


Figure 11: The configuration of  $M^{(1)}$  and  $M^{(2)}$  when  $M^{(2)}$  is in the exterior of  $M^{(1)}$ . The arrows are the  $\hat{n}^{(i)}$  which point into the exterior of each surface. The polyhedra which lie directly on the interior of a given  $M^{(i)}$  are associated with Coxeter group elements of length  $R$ , while the polyhedra which lie directly on the exterior of a given  $M^{(i)}$  are associated with Coxeter group elements of length  $R + 1$ . Although we have drawn  $M^{(1)}$  and  $M^{(2)}$  as circles we are not assuming they are spherical, they could be tori, all we are assuming is that they have a well defined interior and exterior.

along one of the edges touching that vertex. Any loop which passes between adjacent faces which only touch via a common vertex can therefore be continuously deformed into a nearby loop which passes through those faces. Thus we can assume wlog neighbouring faces which contain adjacent sections of  $\mathcal{C}$  share a common edge.

There are four possible ways the polyhedral cells associated to these neighbouring faces could be connected (see Fig. 12 for an illustration):

1. The neighbouring faces are associated with the same polyhedral cell.
2. A pair of neighbouring polyhedral cells share a single common edge.
3. A pair of neighbouring polyhedral cells share a common face (and therefore also common edges).

Case 3 is not possible because, if two polyhedra  $P^{(u')}$  and  $P^{(v')}$  where  $l_S(u') = l_S(v') = r$  meet at a face, there would exist  $s_a \in S$  such that  $l_S(u's_a) = l_S(v') = r = l_S(u')$ , contradicting property (i) of the length function of Coxeter groups (see Section 3.4.2). Therefore, for every pair of neighbouring faces containing adjacent sections of the non-contractible loop, either Case 1 or Case 2 must hold.

The surface of the HQECC at radius  $R - 1$  (which we will denote  $M'$ ) is contained inside  $M$ , where ‘‘inside’’ is well-defined as  $M$  is orientable by Lemma 4.6. Consider continuously deforming  $\mathcal{C}$  so that it lies on  $M'$ , by the following procedure. Take a section of  $\mathcal{C}$  which lies on the faces of a single polyhedral cell,  $P^{(u)}$ , and deform it so that it lies on the faces of  $P^{(u)}$  associated with  $\mathcal{D}_R(u)$  whilst leaving its endpoints unchanged. To see that this can always be done, note that at the edge where faces  $F_a^{(u)}$  and  $F_b^{(v)}$  from two polyhedral cells  $P^{(u)}$  and  $P^{(v)}$  meet (see Fig. 12(b)), the faces  $F_b^{(u)}$  and  $F_a^{(v)}$  are associated with  $\mathcal{D}_R(u)$  by Lemma 4.3ii and iii. The faces of  $P^{(u)}$  associated with  $\mathcal{D}_R(u)$  share common edges, so this deformation can be carried out while leaving the curve intact.

We can repeat this contraction procedure until the loop  $\mathcal{C}$  lies on the faces of  $P^{(I)}$ . At that point we can continuously contract  $\mathcal{C}$  through  $P^{(I)}$  to a point. Therefore every loop on  $M$  can be contracted through the bulk of the tessellation to a point.

Any torus (or connected sum of tori) contains curves which cannot be continuously contracted to a point through the solid torus forming its interior. Therefore  $M$  cannot be homeomorphic to the connected sum of tori. Thus  $M$  is homeomorphic to a 2-sphere.  $\square$

#### 4.2.3 The metric on the boundary surface of the HQECC

We can upper-bound the distance between qudits on the boundary surface by the distance according the word metric between the corresponding elements

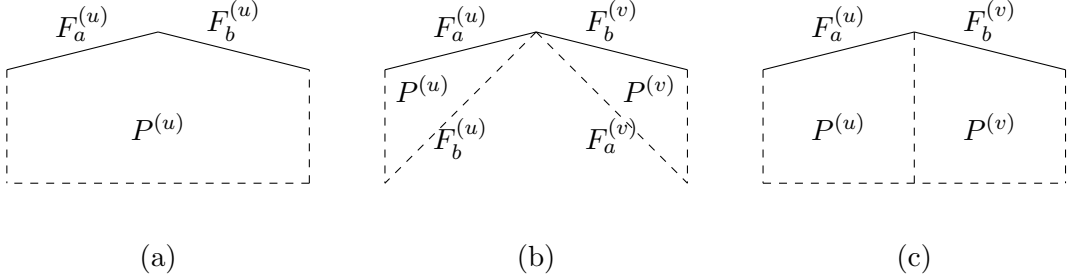


Figure 12: A cross section image of the three possible ways which neighbouring faces in a loop  $\mathcal{C}$  on  $M$  could be connected. In (a) the neighbouring faces are associated with a single polyhedral cell. In (b) neighbouring faces are associated with polyhedral cells which share a single common edge. In (c) the neighbouring faces are associated with polyhedral cells which share a common edge. The figures all represent cross-sections of the tessellations, and in all figures dashed edges represent faces of polyhedra which do not form part of  $M$ , while solid edges represent faces of polyhedra which form part of  $M$ .

of the Coxeter group. Consider two boundary qudits,  $q_a^{(u)}$  and  $q_b^{(v)}$  where  $q_a^{(u)}$  is the qudit associated with the uncontracted tensor leg from the face  $F_a^{(u)}$ , and  $q_b^{(v)}$  is the qudit associated with the uncontracted tensor leg from the face  $F_b^{(v)}$ .

The Coxeter polytopes we use in the HQECC are of size  $O(1)$  in every direction, so the distance between  $q_a^{(u)}$  and  $q_b^{(v)}$  is upper-bounded by  $cd(u, v) = c\ell_S(u^{-1}v)$ , where  $c$  is some constant determined by the size of the Coxeter polytope.

If  $q_a^{(u)}$  and  $q_b^{(v)}$  are nearest-neighbour qudits on the boundary surface of a HQECC then they are separated by distance  $O(1)$ . This follows because the boundary surface of the HQECC is connected, so  $F_a^{(u)}$  and  $F_b^{(v)}$  must share a common edge. The number of Coxeter polyhedra which fit round this edge is upper-bounded by  $m_{ab}$ , so  $\ell_S(u^{-1}v) \leq m_{ab} = O(1)$ .

#### 4.2.4 Operators on the boundary surface of the HQECC

In order to determine the overhead required to simulate the boundary Hamiltonian with a local model we first need to determine the distribution of operator weights that results from pushing the bulk Hamiltonian through the tensor network. In [31] it is shown that an operator  $M$  can be reconstructed on a boundary region  $A$  if  $M$  lies in the greedy entanglement wedge of  $A$ , denoted  $\mathcal{E}[A]$ , where the greedy entanglement wedge is defined as below:

**Definition 12** (Greedy entanglement wedge, definition 8 from [31]). *Suppose*

$A$  is a (not necessarily connected) boundary region. The greedy entanglement wedge of  $A$ , denoted  $\mathcal{E}[A]$ , is the set of bulk points reached by applying the greedy algorithm to all connected components of  $A$  simultaneously.

The greedy algorithm is a simple procedure for finding bulk regions which can be reconstructed on a given boundary region. It constructs the greedy entanglement wedge of a boundary region  $A$  by considering a sequence of cuts  $\{c_\alpha\}$  through the tensor network which are bounded by  $\partial A$  and which correspond to a set of isometries  $\{P_\alpha\}$  from bulk indices to boundary indices. The algorithm begins with the cut  $c_1 = A$ , corresponding to  $P_1 = \mathbb{I}$ . Each cut in the sequence is obtained from the previous one by identifying a (pseudo)-perfect tensor which has at least half of its indices contracted with  $P_\alpha$ , and adding that tensor to  $P_\alpha$  to construct  $P_{\alpha+1}$ . In this way  $P_{\alpha+1}$  is guaranteed to be an isometry if  $P_\alpha$  is. The algorithm terminates when there are no tensors which have at least half their indices contracted with  $P_\alpha$ . (See [31] for details). The greedy algorithm only relies on the properties of perfect tensors, so we can apply it to our HQECC in  $\mathbb{H}^3$ .

A given bulk point will be in the greedy entanglement wedge of many boundary regions. As we are interested in minimising the operator weights of the boundary Hamiltonian we want to calculate the minimum size boundary region that is needed to reconstruct a given bulk operator.

Consider a HQECC described by a perfect tensor,  $T$ , and a Coxeter system  $(W, S)$  with associated Coxeter polyhedra  $P \subseteq \mathbb{H}^3$ . Let the growth rate of  $W$  with respect to  $S$  be  $\tau$ , and let the radius of the HQECC be  $R$ .

By the definition of the growth rate, the number of boundary qudits,  $N$ , will scale as  $O(\tau^R)$ . To reconstruct any operator which acts on the central bulk qudit requires an  $O(1)$  fraction of the boundary qudits, so the number of boundary qudits needed for the reconstruction scales as  $O(\tau^R)$ .<sup>16</sup>

Consider the number of boundary qudits required to reconstruct an operator which acts on a qudit at distance  $x$  from the centre. By assumption we have that  $\mathcal{A}_R(w) > \mathcal{D}_R(w)$  for all  $w \in W$ , and hence for all polyhedral cells in our tessellation of  $\mathbb{H}^3$ . Therefore if we take an operator acting on a qudit at radius  $x$ , and push it through the tensor network, we can push it to the boundary while at each step moving outwards in the tensor network - i.e. we are guaranteed to be able to reconstruct the operator on the boundary using only qudits which are a distance  $R - x$  from the initial qudit, which we will label  $q^{(v)}$ . If we consider shifting the centre of the tensor network to  $q^{(v)}$  we can see that there are  $O(\tau^{R-x})$  qudits which are at distance  $R - x$  from  $q^{(v)}$ . Not all of these lie on the boundary, but we can upper-bound the number of qudits needed for boundary reconstruction by  $O(\tau^{R-x})$ .

---

<sup>16</sup>In theory it is possible to work out the value of the  $O(1)$  constant from the properties of the (pseudo)-perfect tensor and Coxeter system used in a given HQECC, however as we are concerned with asymptotic scaling of weights we don't provide an example of this calculation.

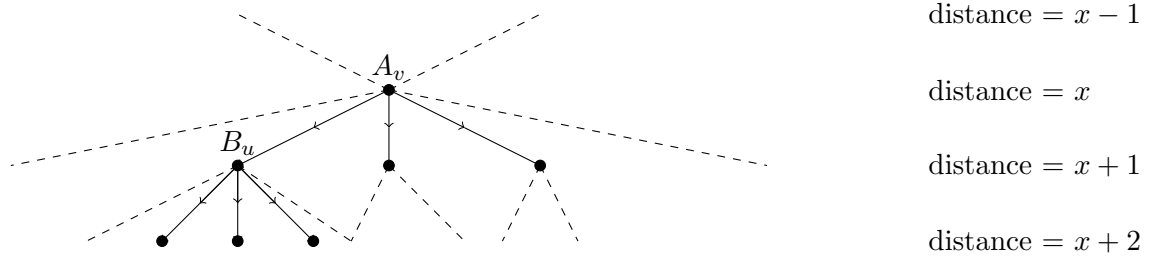


Figure 13: If qudit  $q^{(v)}$  is at distance  $x$  from the centre of the HQECC, and qudit  $q^{(u)}$  is a neighbouring qudit at distance  $x + 1$  from the centre, then an operator  $A_v$  acting on  $q^{(v)}$  can be pushed through  $q^{(u)}$ , so pushing an operator  $A_v \otimes B_u$  where  $B_u$  acts on  $q^{(u)}$  through the tensor network will lead to a boundary operator with the same weight as pushing  $A_v$  alone through the tensor network.

If we consider a geometrically  $k$ -local operator in the bulk, where the deepest qudit the operator acts on is at distance  $x$  from the centre,<sup>17</sup> then the number of qudits needed for boundary reconstruction scales as  $O(\tau^{R-x})$ . To see this consider an operator  $A \otimes B$  where  $A$  acts on qudit  $q^{(v)}$  which is at distance  $x$  from the centre, and  $B$  acts on a neighbouring qudit  $q^{(u)}$  at distance  $x + 1$ , as in Fig. 13. We can reconstruct  $A$  on the boundary by pushing it through  $q^{(u)}$ , therefore the operator  $B$  can necessarily be reconstructed on a subset of the qudits required to reconstruct  $A$ . Hence  $B$  makes no difference to the number of qudits required for boundary reconstruction, and we only need to consider the deepest qudit a given operator acts on. In general there may be more than one deepest qudit, however as  $k$  is constant this can make at most a constant factor difference to the number of qudits needed to reconstruct a given bulk operator.

The number of qudits at distance  $x$  from the centre of the tensor network scales as  $O(\tau^x)$ , so we find that for  $x = 0 : R$  the boundary Hamiltonian has  $O(\tau^x)$  operators of weight  $O(\tau^{R-x})$ . All boundary operators can be chosen to be geometrically  $O(\tau^{R-x})$  local (i.e. the  $O(\tau^{R-x})$  qudits which an operator act on are spread over an  $O(\tau^{-x})$  fraction of the boundary).

#### 4.2.5 A complete holographic duality

In this section we prove our main result: that using a HQECC and simulation techniques from Hamiltonian complexity it is possible to construct a complete holographic duality between 3D hyperbolic space and its 2D boundary.

**Theorem 4.9.** *Let  $\mathbb{H}^3$  denote 3D hyperbolic space, and let  $B_r(x) \subset \mathbb{H}^3$  denote a ball of radius  $r$  centred at  $x$ . Consider any arrangement of  $n$  qudits*

---

<sup>17</sup>Here by deepest operator we mean nearest the centre, so the minimum  $x$ .

in  $\mathbb{H}^3$  such that, for some fixed  $r$ , at most  $k$  qudits and at least one qudit are contained within any  $B_r(x)$ . Let  $L$  denote the minimum radius ball  $B_L(0)$  containing all the qudits (which wlog we can take to be centred at the origin). Let  $H_{\text{bulk}} = \sum_Z h_Z$  be any local Hamiltonian on these qudits, where each  $h_Z$  acts only on qudits contained within some  $B_r(x)$ .

Then we can construct a Hamiltonian  $H_{\text{boundary}}$  on a 2D boundary manifold  $\mathcal{M} \in \mathbb{H}^3$  with the following properties:

1.  $\mathcal{M}$  surrounds all the qudits, has diameter  $O\left(\max(1, \frac{\ln(k)}{r})L + \log \log n\right)$ , and is homeomorphic to the Euclidean 2-sphere.
2. The Hilbert space of the boundary consists of a triangulation of  $\mathcal{M}$  by triangles of  $O(1)$  area, with a qubit at the centre of each triangle, and a total of  $O(n(\log n)^2)$  triangles/qubits.
3. Any local observable/measurement  $M$  in the bulk has a set of corresponding observables/measurements  $\{M'\}$  on the boundary with the same outcome. A local bulk operator  $M$  can be reconstructed on a boundary region  $A$  if  $M$  acts within the greedy entanglement wedge of  $A$ , denoted  $\mathcal{E}[A]$ .
4.  $H_{\text{boundary}}$  consists of 2-local, nearest-neighbour interactions between the boundary qubits. Furthermore,  $H_{\text{boundary}}$  can be chosen to have full local  $SU(2)$  symmetry; i.e. the local interactions can be chosen to all be Heisenberg interactions:  $H_{\text{boundary}} = \sum_{\langle i,j \rangle} \alpha_{ij}(X_i X_j + Y_i Y_j + Z_i Z_j)$ .
5.  $H_{\text{boundary}}$  is a  $(\Delta_L, \epsilon, \eta)$ -simulation of  $H_{\text{bulk}}$  in the rigorous sense of [9, Definition 23], with  $\epsilon, \eta = 1/\text{poly}(\Delta_L)$ ,  $\Delta_L = \Omega\left((\max_Z \|h_Z\|)^{\text{poly}(n \log(n))}\right)$  and  $|\alpha_{ij}| \leq \Delta_L$ .

*Proof.* There are four steps to this simulation:

**Step 1**

The first step is to simulate  $H_{\text{bulk}}$  with a Hamiltonian which acts on the bulk indices of a HQECC in  $\mathbb{H}^3$  of radius  $R = O\left(\max(1, \frac{\ln(k)}{r})L\right)$ .

Note that in a tessellation of  $\mathbb{H}^3$  by Coxeter polytopes the number of polyhedral cells in a ball of radius  $r'$  scales as  $O(\tau^{r'})$ , where we are measuring distances using the word metric,  $d(u, v) = l_S(u^{-1}v)$ . If we want to embed a Hamiltonian  $H_{\text{bulk}}$  in a tessellation we will need to rescale distances between the qudits in  $H_{\text{bulk}}$  so that there is at most one qudit per polyhedral cell of the tessellation. If  $\tau^{r'} = k$ , then  $\frac{r'}{r} = \frac{\ln(k)}{\ln(\tau)r} = O\left(\frac{\ln(k)}{r}\right)$ . If  $\frac{\ln(k)}{r} \geq 1$  then the qudits in  $H_{\text{bulk}}$  are more tightly packed than the polyhedral cells in the tessellation, and we need to rescale the distances between the qudits by a factor of  $O\left(\frac{\ln(k)}{r}\right)$  to ensure there is only one qudit per polyhedral cell of the tessellation. If  $\frac{\ln(k)}{r} < 1$  then the qudits in  $H_{\text{bulk}}$  are less tightly packed

then the polyhedral cells of the tessellation, and we will not need to rescale the distances between qudits.

The radius,  $R$ , of the tessellation needed to contain all the qudits in  $H_{\text{bulk}}$  is then given by:

$$R = \begin{cases} O\left(\frac{\ln(k)}{r}L\right), & \text{if } \frac{\ln(k)}{r} \geq 1 \\ O(L) & \text{otherwise} \end{cases} \quad (89)$$

Once we have rescaled the distances of the qudits in  $H_{\text{bulk}}$  there is at most one qudit per cell of the tessellation. There will be some cells of the tessellation which don't contain any qudits. We can put 'dummy' qudits in these cells - these dummy qudits don't participate in any interactions, so their inclusion is just equivalent to tensoring the Hamiltonian with an identity operator. We can upper and lower bound the number of 'real' qudits in the tessellation. If no cells contain dummy qudits then the number of real qudits in the tessellation is given by  $n_{\text{max}} = N = O(\tau^R)$ , where  $N$  is the number of cells in the tessellation. By assumption there is at least one real qudit in a ball of radius  $r'$ , therefore the minimum number of real qudits in the tessellation scales as  $n_{\text{min}} = O\left(\frac{\tau^R}{\tau^{r'}}\right) = O(\tau^R) = O(N)$ . Therefore  $n = \Theta(\tau^R) = \Theta(N)$ .

If the tessellation of  $\mathbb{H}^3$  by Coxeter polytopes is going to form a HQECC, the Coxeter polytope must have at least 7 faces. We show in Section 4.3 that this bound is achievable, so we will wlog assume the tessellation we are using is by a Coxeter polytope with 7 faces. The perfect tensor used in the HQECC must therefore have 8 indices. Our method to construct perfect tensors can be used to construct perfect tensors with 8 indices for qudits of prime dimension  $p \geq 11$ . Qudits of general dimension  $d$  can be incorporated by embedding qudits into a  $d$ -dimensional subspace of the smallest prime which satisfies both  $p \geq d$  and  $p \geq 11$ . We then add one-body projectors onto the orthogonal complement of these subspaces, multiplied by some  $\Delta'_S \geq |H_{\text{bulk}}|$  to the embedded bulk Hamiltonian. The Hamiltonian,  $H'_{\text{bulk}}$  on the  $n$   $p$ -dimensional qudits is then a perfect simulation of  $H_{\text{bulk}}$ .

We can therefore simulate any  $H_{\text{bulk}}$  which meets the requirements stated in the theorem with a Hamiltonian which acts on the bulk indices of a HQECC in  $\mathbb{H}^3$ .

Now consider simulating  $H_{\text{bulk}}$  with a Hamiltonian  $H_B$  on the boundary surface of the HQECC. The error correction properties of the HQECC ensure that  $H_{\text{bulk}}$  is redundantly encoded on the boundary, so there are a number of Hamiltonians we could choose. Let:

$$H_B = H' \Pi_{\mathcal{C}} + \Delta_S (\mathbb{I} - \Pi_{\mathcal{C}}) \quad (90)$$

where  $H'$  satisfies  $H' \Pi_{\mathcal{C}} = V (H'_{\text{bulk}} \otimes \mathbb{I}_{\text{dummy}}) V^\dagger$ ,  $V$  is the encoding isometry of the HQECC,  $\mathbb{I}_{\text{dummy}}$  acts on the dummy qudits, and  $\Pi_{\mathcal{C}}$  is the projector onto the codespace of the HQECC. Provided  $\Delta_S \geq |H'_{\text{bulk}}|$ ,  $H_B$  meets the

conditions in [9] to be a perfect simulation of  $H'_{\text{bulk}}$ , and (as simulations compose) a perfect simulation of  $H_{\text{bulk}}$ .

There is freedom in this definition as there are many  $H'$  which satisfy the condition stated. We will choose an  $H'$  where every bulk operator has been pushed directly out to the boundary, so that a 1-local bulk operator at radius  $x$  corresponds to a boundary operator of weight  $O(\tau^{R-x})$ . We will also require that the Pauli rank of every bulk operator has been preserved (see Theorem 3.5 for proof we can choose  $H'$  satisfying this condition).

**Step 2**<sup>18</sup>

Having constructed  $H_B$  we now want to simulate it with a geometrically 2-local qudit Hamiltonian using the subdivision and 3-2 gadgets.  $H_B$  has  $O(\tau^x)$  operators of weight  $O(\tau^{R-x})$  for  $x = 0 : R$ . Breaking down a  $k$ -local operator which is a tensor product of operators of the form  $P_A + P_A^\dagger$  to a 2-local operator using the subdivision and 3-2 gadgets requires  $O(k)$  ancillas, and  $O(\log(k))$  rounds of perturbation theory. Therefore it will require a total of:

$$N_a = O\left(\sum_{x=0}^R \tau^x \tau^{R-x}\right) = O(R\tau^R) = O(n \log(n)) \quad (91)$$

ancilla qudits.

The original qudits are in the centre of the polygon-cells which form the boundary.<sup>19</sup> Place the ancilla qudits resulting from this step on the edges of the cells. Each edge then contains  $O(R) = O(\log(n))$  qudits. When breaking down the interactions to 2-local the ancillas are placed nearest the qudits they are interacting with, so none of the resulting 2-local interactions cross more than two of the polygon cells which make up the boundary.

As there are interactions with weights which scale as  $O(n)$  this step requires  $O(\log(n))$  rounds of perturbation theory. By Lemma 3.11,  $r$  rounds of perturbation theory requires  $\Delta$  to scale as  $\Lambda^{6r}$ , so this step requires  $\Delta = \Omega\left((\max_Z ||h_Z||)^{\text{poly}(n)}\right)$ .

**Step 3**

Each of the ancillas introduced in step 2 has degree at most 6. The degree of the original qudits after step 2 is the same as the degree of the original qudits in the initial hypergraph, which can be calculated as:

$$d = \frac{\sum_{x=0}^R \tau^x \tau^{R-x}}{\tau^R} = R \quad (92)$$

Therefore there are  $O(\tau^R)$  qudits of degree  $O(R)$ , and  $O(R\tau^R)$  qudits of degree  $O(1)$ . We reduce the degree of each vertex to at most  $3(p-1)$  in the following manner:

---

<sup>18</sup>In steps 2 and 3 we are following the methods developed in [30], replacing the qubit perturbation gadgets with qudit perturbation gadgets, and making use of the structure of the interaction graph on the boundary.

<sup>19</sup>The polygon cells are the faces of the tensor network which correspond to the uncontracted tensor indices.

- i. Use the subdivision gadget to localise each qudit with degree  $O(R)$ , this requires  $O(R)$  ancilla qudits per polygon cell of the boundary, so  $O(R\tau^R)$  ancilla qudits for the entire boundary
- ii. Apply the triangle gadget to each qudit to reduce the degree to  $3(p-1)$ , by pairing edges of the form  $P_a + P_a^\dagger$  in parallel. Reducing the degree of one  $O(R)$  degree vertex in this manner requires  $O(\log(R))$  rounds of perturbation theory, and  $O(R)$  ancillas. Therefore applying this step to the entire graph requires  $O(R\tau^R)$  ancillas.

Once the degree of each qudit has been reduced there are  $O(R)$  qudits in each of the polygon cells of the boundary.

Finally we need to remove all the crossings using crossing gadgets. Each interaction is constrained to 2 of the polygon cells which make up the boundary surface, so we can consider each polygon cell and its adjacent cells separately.<sup>20</sup> There are  $O(R)$  qudits, and hence at most  $O(R^2)$  interactions in each polygon cell, including contributions from adjacent cells. Therefore there are at most  $O(R^2)$  crossings. We use the subdivision gadget to localise each crossing,<sup>21</sup> then apply the crossing gadget in parallel to each localised crossing. This requires  $O(R^2)$  ancillas per polygon cell of the boundary surface, so requires  $O(R^2\tau^R) = O(n \log(n)^2)$  ancilla qudits. These ancilla qudits are placed within the corresponding face of the boundary surface.

This step required  $O(\log \log n)$  rounds of perturbation theory, so we require  $\Delta$  to scale as  $\Delta = \Omega((\max_Z ||h_Z||)^{\text{poly}(n \log(n))})$

Label the Hamiltonian resulting from this step as  $H'_B$ .

#### Step 4

Finally we simulate  $H'_B$  with a qubit  $\{XX + YY + ZZ\}$ -Hamiltonian on a  $2d$  lattice,  $H_{\text{boundary}}$ . First use the technique from Lemma 21 in [9] to simulate  $H'_B$  with a qubit Hamiltonian by simulating each qudit with  $\lceil \log_2 p \rceil$  qubits. The resulting Hamiltonian is given by:

$$H''_B = \mathcal{E}(H'_B) + \Delta_4 \sum_{i=0}^{n'} P_i \quad (93)$$

where  $\mathcal{E}(M) = VMV^\dagger$ ,  $V = W^{\otimes n'}$ ,<sup>22</sup>  $W$  is an isometry  $W : \mathbb{C}^d \rightarrow (\mathbb{C}^2)^{\otimes \lceil \log_2 p \rceil}$ , and  $P = \mathbb{I} - WW^\dagger$ . This requires  $n' \lceil \log_2 p \rceil = O(n')$  qubits.

The operators in  $H''_B$  are at most  $2\lceil \log_2 p \rceil$ -local, and the qubits have degree at most  $3(p-1)\lceil \log_2 p \rceil$ .

<sup>20</sup>This will double count some crossings as each cell will be included when considering its adjacent cells too, but as we are only interested in the asymptotic scaling this double-counting is not important.

<sup>21</sup>This step can be skipped for edges with only one crossing, where each qudit involved in the crossing interactions has degree at most  $3(p-1)$ .

<sup>22</sup> $n'$  is the total number of qudits in  $H'_B$ .

Next we use the technique from [9, Lemma 22] to simulate  $H_B''$  with a real Hamiltonian. This is a perfect simulation, which requires  $2N' = O(n')$  qubits, it increases the locality of the interactions to at most  $4\lceil\log_2 p\rceil = O(1)$  and doesn't change the degree of the qubits.

Using the technique from [9, Lemma 39] we can then simulate the real Hamiltonian with a Hamiltonian containing no  $Y$  operators. This involves adding an ancilla qubit for every interaction in the Hamiltonian. As each qubit is involved in a fixed number of interactions, this only requires  $O(n')$  ancilla qubits, so the total number of qubits involved in the Hamiltonian is still  $O(n')$ . The locality of each interaction in the Hamiltonian is increased by 1. This requires  $O(1)$  rounds of perturbation theory.

The qubit subdivision and 3-2 perturbation gadgets from [30] can then be used to reduce the Hamiltonian containing no  $Y$ s to a 2-local Pauli interaction with no  $Y$ s, leaving a Hamiltonian of the form  $\sum_{i>j} \alpha_{ij} A_{ij} + \sum_k (\beta_k X_k + \gamma_k Z_k)$  where  $A_{ij}$  is one of  $X_i X_j$ ,  $X_i Z_j$ ,  $Z_i X_j$  or  $Z_i Z_j$  [9, Lemma 39]. This requires  $O(1)$  rounds of perturbation theory, and  $O(n')$  ancilla qubits.

Next we use the subspace perturbation gadget from [9, Lemma 41] to simulate the Hamiltonian of the form  $\sum_{i>j} \alpha_{ij} A_{ij} + \sum_k (\beta_k X_k + \gamma_k Z_k)$  with a  $\{XX + YY + ZZ\}$ -Hamiltonian. This requires encoding one logical qubit in four physical qubits, so introduces  $O(N')$  ancilla qubits, and requires  $O(1)$  rounds of perturbation theory.

Finally, we can simulate the general  $\{XX + YY + ZZ\}$ -Hamiltonian with a  $\{XX + YY + ZZ\}$ -Hamiltonian on a triangulation of the boundary surface of the HQECC using the perturbation gadgets from [32]. These perturbation gadgets are generalisations of the fork, crossing and subdivision gadgets from [30] which use a pair of mediator qubits, rather than a single ancilla qubit, so that all interactions in the final Hamiltonian are of the form  $\{XX + YY + ZZ\}$ . Following the method in [32], first reduce the degree of all vertices in the interaction graph to 3 using the subdivision and fork gadgets. This requires  $O(1)$  ancillas and  $O(1)$  rounds of perturbation theory per qubit, and can be done to all qubits in the Hamiltonian in parallel. Next remove all the crossings. The qudit Hamiltonian  $H_B'$  had no crossings, and our simulation of  $H_B'$  with a  $\{XX + YY + ZZ\}$ -Hamiltonian will have introduced  $O(1)$  crossings per qudit in  $H_B'$ , so  $O(n')$  crossings across the entire interaction graph. The crossings are localised using the subdivision gadget, then removed using the crossing gadget. This requires  $O(n')$  ancilla qubits.

Step 4 therefore requires a total of  $O(n') = O(n \log(n)^2)$  qubits. The scaling of  $\Delta$  is unchanged by this final step as it only required  $O(1)$  rounds of perturbation theory.

Each qubit has degree at most 3, so we can construct a triangulation of the boundary surface with a qubit in the centre of each triangle. This is not an  $O(1)$  triangulation, but if we increase the diameter of our boundary

manifold to  $O\left(\max(1, \frac{\ln(k)}{r})L + \log \log n\right)$  then we can construct an  $O(1)$  triangulation with a qubit in the centre of each triangle (this follows because we are working in hyperbolic space). This surface will be homeomorphic to a sphere as boundary surface of the HQECC is homeomorphic to a sphere by Lemma 4.8.

The final Hamiltonian,  $H_{\text{boundary}}$ , is a  $(\Delta_L, \epsilon, \eta)$ -simulation of  $H_{\text{bulk}}$  with full local  $\text{SU}(2)$  symmetry. The total number of qubits required scales as  $O\left(n \log(n)^2\right)$ , and  $\Delta_L = \Omega\left((\max_Z ||h_Z||)^{\text{poly}(n \log(n))}\right)$ . The perturbation gadget techniques require that  $\epsilon, \eta = 1/\text{poly}(\Delta_L)$ . The coupling strengths in  $H_{\text{boundary}}$ ,  $\alpha_{ij}$ , are upper bounded by  $\Delta_L$ .<sup>23</sup>

It is immediate from the definition of the greedy entanglement wedge [31, Definition 8] that bulk local operators in  $\mathcal{E}(A)$  can be reconstructed on  $A$ . The boundary observables / measurements  $\{M'\}$  corresponding to a bulk observable / measurement  $M$  have the same outcome because simulations preserve the outcome of all measurements.

□

Note that the fact that  $H_{\text{boundary}}$  is a  $(\Delta_L, \epsilon, \eta)$ -simulation  $H_{\text{bulk}}$  immediately implies, by results of [9], that the partition function, time dynamics, and all other physics of the boundary is the same as that of the bulk, up to  $O(1/\text{poly}(\epsilon, \eta))$  errors which can be made as small as desired by increasing  $\Delta_L$ . (See [9] for the precise mathematical statements.)

### 4.3 HQECC constructed from pentagonal prisms

The proof of Theorem 4.9 does not require any particular HQECC - all it requires is that one exists. Here and in Section 4.4 we provide examples of two pairs of Coxeter group and tensor which can be used to construct a HQECC. There are many more which could be constructed.

First we construct a HQECC using a perfect tensor, and a non-uniform Coxeter polytope. The Coxeter polytope,  $P_1$ , we use is a pentagonal prism. It is described by the Coxeter diagram,  $\Sigma(P_1)$ , shown in Fig. 14. The elliptic subdiagrams of  $\Sigma(P_1)$  are shown in Table 2.<sup>24</sup>

The maximum  $|J|$  such that  $W_J$  is finite is three, so  $|\mathcal{D}_R(w)| \leq 3 \forall w \in W$ . Clearly if we construct a perfect tensor with 8 legs, and place one tensor in each polyhedral-cell in a tessellation of  $\mathbb{H}^3$  by pentagonal prisms then the tensor network will be a HQECC. Details of the tensor are given in Section 4.3.1.

---

<sup>23</sup>In steps 2 and 3 we assume that all operators are Pauli rank 2 operators of the form  $P_A + P_A^\dagger$ . We have shown that the HQECC preserves the Pauli rank of operators (Theorem 3.5), so accounting for operators of general form will only increase the overheads calculated by a constant factor.

<sup>24</sup>Elliptic subdiagrams are subdiagrams containing  $J \subseteq S$  such that  $W_J$  is finite.

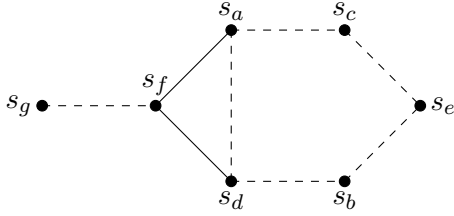


Figure 14: Coxeter diagram,  $\Sigma(P_1)$ , for the Coxeter group associated with the pentagonal prism. The vertices of the graph are labelled with the corresponding generator of the Coxeter group. The faces  $F_f$  and  $F_g$  of the Coxeter polyhedra (corresponding to the generators  $s_f$  and  $s_g$ ) are the pentagonal faces of the prism, the faces  $F_a - F_e$  are the quadrilateral faces.

Name	Diagram	Generating sets
$A_1$	•	$\{s_a\}, \{s_b\}, \{s_c\}, \{s_d\}, \{s_e\}, \{s_f\}, \{s_g\}$
$A_1 \times A_1$	• •	$\{s_a, s_b\}, \{s_a, s_e\}, \{s_a, s_g\}, \{s_b, s_c\}, \{s_b, s_f\}, \{s_b, s_g\}, \{s_c, s_d\}, \{s_c, s_f\}, \{s_c, s_g\}, \{s_d, s_e\}, \{s_d, s_g\}, \{s_e, s_f\}, \{s_e, s_g\}$
$A_2$ (equivalently $I_2^{(3)}$ )	• — •	$\{s_a, s_f\}, \{s_d, s_f\}$
$A_1 \times A_1 \times A_1$	• • •	$\{s_a, s_e, s_g\}, \{s_a, s_b, s_g\}, \{s_c, s_d, s_g\}, \{s_d, s_e, s_g\}, \{s_b, s_c, s_f\}, \{s_b, s_c, s_g\}$
$A_2 \times A_1$	• — • •	$\{s_a, s_b, s_f\}, \{s_a, s_e, s_f\}, \{s_c, s_d, s_f\}, \{s_d, s_e, s_f\}$

Table 2: Elliptic subdiagrams of  $\Sigma(P_1)$ .

The growth rate of the Coxeter group is 3.13.<sup>25</sup>

#### 4.3.1 Perfect tensor

We construct a AME(8, 11) stabilizer state via a classical Reed Solomon code with  $n = 8, k = 4$  over  $\mathbb{Z}_{11}$  defined by the set  $S = \{1, 2, 3, 4, 5, 6, 7, 8\} \in \mathbb{Z}_{11}$ . The generator matrix is given by:

$$G = \begin{pmatrix} 1 & 1 & 1 & 1 & 1 & 1 & 1 & 1 \\ 1 & 2 & 3 & 4 & 5 & 6 & 7 & 8 \\ 1 & 4 & 9 & 5 & 3 & 3 & 5 & 9 \\ 1 & 8 & 5 & 9 & 4 & 7 & 2 & 6 \end{pmatrix} \quad (94)$$

In standard form this becomes:

---

<sup>25</sup>The growth rate was calculated using CoxIterWeb [18], a web applet which computes invariants of Coxeter groups.

$$G = \begin{pmatrix} 1 & 0 & 0 & 0 & 10 & 7 & 1 & 2 \\ 0 & 1 & 0 & 0 & 4 & 4 & 3 & 4 \\ 0 & 0 & 1 & 0 & 5 & 2 & 10 & 4 \\ 0 & 0 & 0 & 1 & 4 & 10 & 9 & 2 \end{pmatrix} \quad (95)$$

Giving a parity check matrix:

$$H = \begin{pmatrix} 1 & 7 & 6 & 7 & 1 & 0 & 0 & 0 \\ 4 & 7 & 9 & 1 & 0 & 1 & 0 & 0 \\ 10 & 8 & 1 & 2 & 0 & 0 & 1 & 0 \\ 9 & 7 & 7 & 9 & 0 & 0 & 0 & 1 \end{pmatrix} \quad (96)$$

The stabilizer generators of the AME(8, 11) stabilizer state are then given by:

$$M = \left( \begin{array}{cccccccc|cccccccccc} 1 & 0 & 0 & 0 & 10 & 7 & 1 & 2 & 0 & 0 & 0 & 0 & 0 & 0 & 0 & 0 \\ 0 & 1 & 0 & 0 & 4 & 4 & 3 & 4 & 0 & 0 & 0 & 0 & 0 & 0 & 0 & 0 \\ 0 & 0 & 1 & 0 & 5 & 2 & 10 & 4 & 0 & 0 & 0 & 0 & 0 & 0 & 0 & 0 \\ 0 & 0 & 0 & 1 & 4 & 10 & 9 & 2 & 0 & 0 & 0 & 0 & 0 & 0 & 0 & 0 \\ 0 & 0 & 0 & 0 & 0 & 0 & 0 & 0 & 1 & 7 & 6 & 7 & 1 & 0 & 0 & 0 \\ 0 & 0 & 0 & 0 & 0 & 0 & 0 & 0 & 4 & 7 & 9 & 1 & 0 & 1 & 0 & 0 \\ 0 & 0 & 0 & 0 & 0 & 0 & 0 & 0 & 10 & 8 & 1 & 2 & 0 & 0 & 1 & 0 \\ 0 & 0 & 0 & 0 & 0 & 0 & 0 & 0 & 9 & 7 & 7 & 9 & 0 & 0 & 0 & 1 \end{array} \right) \quad (97)$$

The tensor which describes the stabilizer state is a perfect tensor.

#### 4.4 HQECC based on the order-4 dodecahedral honeycomb

The next HQECC we consider is constructed using pseudo-perfect tensors. There are only four compact, regular honeycombings of  $\mathbb{H}^3$ , and all the honeycombings are by polyhedra with even number of faces, so to use any of them in a HQECC would require a pseudo-perfect tensor. Here we use the order-4 dodecahedral honeycomb.

The Coxeter polytope,  $P_2$ , we use is right angled dodecahedron. It is described by the Coxeter diagram,  $\Sigma(P_2)$ , shown in Fig. 15. The elliptic subdiagrams of  $\Sigma(P_2)$  are shown in Table 3.

The maximum  $|J|$  such that  $W_J$  is finite is three, so  $|\mathcal{D}_R(w)| \leq 3 \forall w \in W$ . Clearly if we construct a pseudo-perfect tensor with 13 legs, and place one tensor in each polyhedral-cell in a tessellation of  $\mathbb{H}^3$  by right-angled dodecahedra then the tensor network will be a HQECC. Details of the tensor are given in Section 4.4.1.

The growth rate of the Coxeter group is 7.87.<sup>26</sup>

---

<sup>26</sup>The growth rate was calculated using CoxIterWeb [18], a web applet which computes invariants of Coxiter groups.

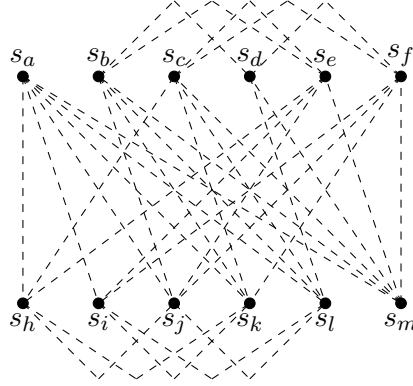


Figure 15: Coxeter diagram,  $\Sigma(P_2)$ , for the Coxeter group associated with order-4 dodecahedral honeycomb. Each pentagonal face of a dodecahedral cell has a dihedral angle of  $\frac{\pi}{2}$  with the five faces it intersects, and diverges from the other six faces of the dodecahedron.

Name	Diagram	Generating sets
$A_1$	•	$\{s_a\}, \{s_b\}, \{s_c\}, \{s_d\}, \{s_e\}, \{s_f\}, \{s_g\}, \{s_h\}, \{s_i\}, \{s_j\}, \{s_k\}, \{s_l\}$
$A_1 \times A_1$	•   •	$\{s_a, s_b\}, \{s_a, s_c\}, \{s_a, s_d\}, \{s_a, s_e\}, \{s_a, s_f\}, \{s_b, s_c\}, \{s_b, s_f\}, \{s_b, s_g\}, \{s_b, s_h\}, \{s_c, s_d\}, \{s_c, s_h\}, \{s_c, s_i\}, \{s_d, s_e\}, \{s_d, s_i\}, \{s_d, s_j\}, \{s_e, s_f\}, \{s_e, s_j\}, \{s_e, s_k\}, \{s_f, s_k\}, \{s_f, s_g\}, \{s_g, s_l\}, \{s_g, s_h\}, \{s_g, s_k\}, \{s_h, s_l\}, \{s_h, s_i\}, \{s_i, s_j\}, \{s_i, s_l\}, \{s_j, s_l\}, \{s_j, s_k\}, \{s_k, s_l\}$
$A_1 \times A_1 \times A_1$	•   •   •	$\{s_a, s_b, s_c\}, \{s_a, s_c, s_d\}, \{s_a, s_d, s_e\}, \{s_a, s_e, s_f\}, \{s_a, s_f, s_b\}, \{s_b, s_f, s_g\}, \{s_b, s_c, s_h\}, \{s_b, s_g, s_h\}, \{s_c, s_h, s_i\}, \{s_c, s_d, s_i\}, \{s_d, s_e, s_j\}, \{s_d, s_i, s_j\}, \{s_e, s_f, s_k\}, \{s_e, s_j, s_k\}, \{s_f, s_g, s_k\}, \{s_g, s_k, s_l\}, \{s_g, s_h, s_l\}, \{s_h, s_i, s_l\}, \{s_i, s_j, s_l\}, \{s_j, s_k, s_l\}$

Table 3: Elliptic subdiagrams of  $\Sigma(P_2)$ .

#### 4.4.1 Pseudo-perfect tensor

We construct a AME(13, 13) stabilizer state via a classical Reed Solomon code with  $n = 13, k = 6$  over  $\mathbb{Z}_{13}$  defined by the set  $S = \{0, 1, 2, 3, 4, 5, 6, 7, 8, 9, 10, 11, 12\} \in \mathbb{Z}_{13}$ . The generator matrix is given by:

$$G = \begin{pmatrix} 1 & 1 & 1 & 1 & 1 & 1 & 1 & 1 & 1 & 1 & 1 & 1 & 1 \\ 0 & 1 & 2 & 3 & 4 & 5 & 6 & 7 & 8 & 9 & 10 & 11 & 12 \\ 0 & 1 & 4 & 9 & 3 & 12 & 10 & 10 & 12 & 3 & 9 & 4 & 1 \\ 0 & 1 & 8 & 1 & 12 & 8 & 8 & 5 & 5 & 1 & 12 & 5 & 12 \\ 0 & 1 & 3 & 3 & 9 & 1 & 9 & 9 & 1 & 9 & 3 & 3 & 1 \\ 0 & 1 & 6 & 9 & 10 & 5 & 2 & 11 & 8 & 3 & 4 & 7 & 12 \end{pmatrix} \quad (98)$$

In standard form this becomes:

$$G = \begin{pmatrix} 1 & 0 & 0 & 0 & 0 & 0 & 12 & 7 & 5 & 9 & 4 & 8 & 6 \\ 0 & 1 & 0 & 0 & 0 & 0 & 6 & 9 & 3 & 3 & 11 & 8 & 11 \\ 0 & 0 & 1 & 0 & 0 & 0 & 11 & 7 & 6 & 8 & 11 & 1 & 7 \\ 0 & 0 & 0 & 1 & 0 & 0 & 7 & 1 & 11 & 8 & 6 & 7 & 11 \\ 0 & 0 & 0 & 0 & 1 & 0 & 11 & 8 & 11 & 3 & 3 & 9 & 6 \\ 0 & 0 & 0 & 0 & 0 & 1 & 6 & 8 & 4 & 9 & 5 & 7 & 12 \end{pmatrix} \quad (99)$$

Giving a parity check matrix:

$$H = \begin{pmatrix} 1 & 7 & 2 & 6 & 2 & 7 & 1 & 0 & 0 & 0 & 0 & 0 & 0 \\ 6 & 4 & 6 & 12 & 5 & 5 & 0 & 1 & 0 & 0 & 0 & 0 & 0 \\ 8 & 10 & 7 & 2 & 2 & 9 & 0 & 0 & 1 & 0 & 0 & 0 & 0 \\ 4 & 10 & 5 & 5 & 10 & 4 & 0 & 0 & 0 & 1 & 0 & 0 & 0 \\ 9 & 2 & 2 & 7 & 10 & 8 & 0 & 0 & 0 & 0 & 1 & 0 & 0 \\ 5 & 5 & 12 & 6 & 4 & 6 & 0 & 0 & 0 & 0 & 0 & 1 & 0 \\ 7 & 2 & 6 & 2 & 7 & 1 & 0 & 0 & 0 & 0 & 0 & 0 & 1 \end{pmatrix} \quad (100)$$

The stabilizer generators of the AME(13, 13) state are given by:

$$M = \left( \begin{array}{cccccccc|cccccccccccc} 1 & 0 & 0 & 0 & 0 & 0 & 12 & 7 & 5 & 9 & 4 & 8 & 6 & 0 & 0 & 0 & 0 & 0 & 0 & 0 & 0 & 0 & 0 & 0 \\ 0 & 1 & 0 & 0 & 0 & 0 & 6 & 9 & 3 & 3 & 11 & 8 & 11 & 0 & 0 & 0 & 0 & 0 & 0 & 0 & 0 & 0 & 0 & 0 & 0 \\ 0 & 0 & 1 & 0 & 0 & 0 & 11 & 7 & 6 & 8 & 11 & 1 & 7 & 0 & 0 & 0 & 0 & 0 & 0 & 0 & 0 & 0 & 0 & 0 & 0 \\ 0 & 0 & 0 & 1 & 0 & 0 & 7 & 1 & 11 & 8 & 6 & 7 & 11 & 0 & 0 & 0 & 0 & 0 & 0 & 0 & 0 & 0 & 0 & 0 & 0 \\ 0 & 0 & 0 & 0 & 1 & 0 & 11 & 8 & 11 & 3 & 3 & 9 & 6 & 0 & 0 & 0 & 0 & 0 & 0 & 0 & 0 & 0 & 0 & 0 & 0 \\ 0 & 0 & 0 & 0 & 0 & 1 & 6 & 8 & 4 & 9 & 5 & 7 & 12 & 0 & 0 & 0 & 0 & 0 & 0 & 0 & 0 & 0 & 0 & 0 & 0 \\ 0 & 0 & 0 & 0 & 0 & 0 & 0 & 0 & 0 & 0 & 0 & 0 & 0 & 1 & 7 & 2 & 6 & 2 & 7 & 1 & 0 & 0 & 0 & 0 & 0 \\ 0 & 0 & 0 & 0 & 0 & 0 & 0 & 0 & 0 & 0 & 0 & 0 & 0 & 6 & 4 & 6 & 12 & 5 & 5 & 0 & 1 & 0 & 0 & 0 & 0 \\ 0 & 0 & 0 & 0 & 0 & 0 & 0 & 0 & 0 & 0 & 0 & 0 & 0 & 8 & 10 & 7 & 2 & 2 & 9 & 0 & 0 & 1 & 0 & 0 & 0 \\ 0 & 0 & 0 & 0 & 0 & 0 & 0 & 0 & 0 & 0 & 0 & 0 & 0 & 4 & 10 & 5 & 5 & 10 & 4 & 0 & 0 & 0 & 1 & 0 & 0 \\ 0 & 0 & 0 & 0 & 0 & 0 & 0 & 0 & 0 & 0 & 0 & 0 & 0 & 9 & 2 & 2 & 7 & 10 & 8 & 0 & 0 & 0 & 0 & 1 & 0 \\ 0 & 0 & 0 & 0 & 0 & 0 & 0 & 0 & 0 & 0 & 0 & 0 & 0 & 5 & 5 & 12 & 6 & 4 & 6 & 0 & 0 & 0 & 0 & 0 & 1 \\ 0 & 0 & 0 & 0 & 0 & 0 & 0 & 0 & 0 & 0 & 0 & 0 & 0 & 7 & 2 & 6 & 2 & 7 & 1 & 0 & 0 & 0 & 0 & 0 & 1 \end{array} \right) \quad (101)$$

The tensor which describes the AME(13,13) stabilizer state is a pseudo-perfect tensor.

## 5 Discussion

### 5.1 Main result

In our bulk/boundary mapping, local Hamiltonians in 3D hyperbolic space,  $\mathbb{H}^3$ , are mapped to local Hamiltonians on its boundary. At first glance this may appear to be at odds with the bulk reconstruction expected in AdS/CFT, where observables deep in the bulk are expected to map to non-local observables on the boundary CFT. However, while the local simulation in our construction ensures that the boundary *Hamiltonian* is local, it does not affect the locality of *observables*. As in the HaPPY code, observables deep in the bulk in our construction map to observables which require a large fraction of the boundary to be reconstructed, while observables near the boundary of the HQECC can be reconstructed on smaller fractions of the boundary (see point 3 from Theorem 4.9 for details).

Furthermore, point 1 from Theorem 4.9 demonstrates that the boundary surface in our construction really is a boundary geometrically. The radius of the boundary surface is at a distance  $\log \log n$  from the  $n$  bulk qudits. In Section 5.3 we compare this with the spherical and Euclidean case.

Point 4 from Theorem 4.9, which follows immediately from work in [9], says that we can always chose that the boundary Hamiltonian in our holographic duality has full local  $SU(2)$  symmetry. This suggests that it may be possible to systematically incorporate local symmetries into the construction, such as gauge symmetries. Doing so would involve tailoring our general construction to specific bulk models of interest, and is an interesting future avenue.

Finally it is worth commenting on the energy scales in the construction. There are two large energy scales. The first  $\Delta_S$  is the energy penalty applied to boundary states which violate stabilizers of the HQECC. In Section 5.2 we discuss the significance of this energy scale. The second large energy scale,  $\Delta_L$ , is the energy scale at which the local simulation of point 5 from Theorem 4.9 breaks down. At energies above  $\Delta_L$  there is no longer any meaningful duality between bulk and boundary.

### 5.2 Black hole formation in HQECC

In [31] it is suggested that black holes can be incorporated into HQECC models of AdS/CFT by removing tensors from the tensor network. If a tensor is removed from the bulk of a HQECC then the tensor's one logical index is replaced by  $t-1$  logical indices, corresponding to the legs that were previously contracted with the missing tensor. This increases the code subspace of the

boundary Hilbert space, and in [31] it is suggested that this increased code space can be interpreted as describing bulk configurations which contain a black hole. It is noted in [31] that this model ensures that every boundary state is dual to a bulk state, and that black hole entropy scales with area, as expected from the Beckenstein-Hawking bound [5, 20]. By extending the toy models of holographic duality to encompass Hamiltonians we can extend this to consider toy models of black hole *formation*. We can gain a qualitative picture of the boundary dynamics dual to black hole formation in the bulk from general considerations, even without considering a specific, discretised, toy model model of gravity in the bulk.

Consider a HQECC, where the bulk Hamiltonian is some local Hamiltonian which models semi-classical gravity given by  $H_{\text{bulk}} = \sum_Z h_Z$ . Choose  $\Delta_S$  such that  $\Delta_S \gg \|h_Z\|$ , but  $\Delta_S < \sum_Z \|h_Z\|$ .<sup>27</sup> To model a shell of in-falling matter in the bulk, we can start from the vacuum state (the ground state) and apply local operators to a shell of bulk qudits near the boundary. Each local excitation will pick up energy from only a few of the local  $h_Z$  terms, but the overall state will have large energy from summing over all these contributions. Thus, for suitable  $\Delta_S$ , the total energy of this configuration will be greater than  $\Delta_S$ , but these local excitations still correspond to a boundary state which is within the code space.

If we assume that under the action of  $H_{\text{bulk}}$  this shell of matter collapses inwards towards the centre of the HQECC (as would be expected from a Hamiltonian that models gravity), then the bulk will unitarily evolve to a configuration where most regions are in a low energy state (with respect to the Hamiltonians that act there), and most of the energy comes from a few terms near the centre of the HQECC. The evolution of the bulk has been unitary, so the energy of the system is still greater than  $\Delta_S$ . But by assumption  $\Delta_S \gg \|h_Z\|$ , so it is not possible for the bulk to pick up energy greater than  $\Delta_S$  from only a few  $h_Z$  terms.

The only other way the system can pick up energy greater than  $\Delta_S$  is by violating one of the stabilizers of the HQECC. On the boundary it is clear that if we begin in a state with energy greater than  $\Delta_S$  it is possible to unitarily evolve to a state which is outside the code space and violates a stabilizer. But in the bulk it is not meaningful to talk about violating a stabilizer, as the stabilizers do not act on the same Hilbert space as the bulk logical indices. If, however, one of the bulk tensors has been removed, as in the models of black holes from [31], then the stabilizers corresponding to the removed tensor *do* act on the Hilbert space of the  $t - 1$  new logical indices, and it is meaningful to talk about these stabilizers being violated. The only way for the system to conserve energy under these dynamics is

---

<sup>27</sup>Recall  $\Delta_S$  is the energy penalty given to boundary states which violate stabilizer terms. It is distinct from  $\Delta_L$ , which is the energy scale at which the local simulation breaks down. For the purposes of this discussion we can take  $\Delta_L = \infty$ , so we only need to consider one large energy scale.

for the tensor network to be ‘broken’, and for at least one of the stabilizers corresponding to the missing tensor to be violated. This process therefore predicts the formation of a toy model black hole as proposed in [31].

It also follows from this discussion that the toy models of black holes correspond to high energy states on the boundary, which pick up their energy from a small number of high energy terms in the Hamiltonian.

Therefore, with an appropriately chosen bulk Hamiltonian, we can model black hole formation in our HQECC. No information is lost in this process (as the dynamics are unitary we can always reverse them), but the isometry which takes bulk states to boundary states will have changed, so the ‘dictionary’ for reconstructing the bulk state from the boundary state will be different. In particular, the fraction of the boundary needed to reconstruct an operator acting on the central bulk region will increase in the presence of a toy model black hole.

To see this consider a central black hole where one tensor is removed from the HQECC. An operator which acts on the degrees of freedom representing the black hole acts on all  $t - 1$  of the logical indices, so will need to be pushed through all of the  $t - 1$  tensors at radius 1 in the HQECC. In the absence of any black hole an operator acting on the central bulk index could be reconstructed via pushing through just  $\lceil \frac{t}{2} \rceil$  of the tensors at radius 1 in the HQECC. So the fraction of the boundary needed for bulk reconstruction of the centre increases in the presence of a central black hole.

Throughout this discussion we have concentrated on a black hole in the centre of the bulk for clarity, but these qualitative conclusions apply equally well to black holes situated at any point in the bulk.

### 5.3 Other geometries

In this paper we have constructed a complete duality between  $\mathbb{H}^3$  and its 2D boundary as a toy model for a duality between Anti-de Sitter space and its boundary. From a cosmological perspective it would also be interesting to consider toy models of dualities between positively curved / flat geometries, and their boundaries.

There is no reason to suspect that the error correcting properties of AdS/CFT should be recreated in such dualities, so it is not clear that the error correcting code constructions of HQECC will be relevant. However, the theory of simulation from [9] can be applied in any geometry, and it follows immediately from the results in [9] that it is possible to construct a complete duality between Euclidean / spherical geometry in dimension 3, and a 2D ‘boundary’ surface. However, it is not clear whether such a ‘boundary’ surface can be considered a geometric boundary in any meaningful sense.

In Euclidean geometry, results from [9] imply that in order to simulate  $n$  bulk qudits in  $\mathbb{E}^3$  with a local boundary model requires  $O(\text{poly}(n))$  boundary qudits. If we maintain the density of qudits from the bulk on the boundary

this implies that if the bulk qudits were contained in a ball of radius  $R$ , then the boundary surface would be at a radius  $R' = O(R + \text{poly}(n))$ , so the distance between the bulk qudits and the boundary surface would increase polynomially rapidly with  $n$ .

The situation in the positively curved case is worse.  $\mathbb{S}^3$  is finite, so the boundary surface required to simulate  $n$  qudits which lie in  $\mathbb{S}^3$  might not itself lie in  $\mathbb{S}^3$ .

Therefore, while it is possible to construct a complete duality between  $\mathbb{E}^3$  or  $\mathbb{S}^3$  and a 2D surface, it is not clear that such a duality could be considered a bulk / boundary mapping.

## 6 Conclusions

Even in the absence of a useful duality at the level of Hamiltonians, holographic quantum codes such as [31] already provide a simple, tractable toy model many of the interesting static features expected of the real AdS/CFT “dictionary”. Such as redundant encoding and complementary recovery of information on the boundary [3, 19], entropic relations such as the Ryu-Takayanagi formula [35, 36], and even toy models of (static) black holes satisfying the Beckenstein-Hawking bound [5, 20]. However, without a useful holographic mapping between Hamiltonians, these toy models give more limited insight into the relationship between bulk and boundary energy scales – a key aspect of AdS/CFT, where non-classical bulk spacetime geometries are believed to correspond to high-energy boundary state. More importantly, without a corresponding duality on Hamiltonians, we cannot say how dynamics in the bulk is reflected in the boundary.

By extending the toy models of holographic duality to encompass Hamiltonians, we show one way to complete this “dictionary”. For example, it follows almost immediately from our construction that the toy models of static black holes proposed in [31] do indeed correspond to high-energy states of the local boundary model, which moreover pick up their energy from a small number of high energy-terms in the boundary Hamiltonian.

More intriguingly, our construction allows these toy models to say something about how dynamics in the bulk is reflected in the boundary. Even without writing down any specific local bulk Hamiltonian, the structure of the bulk/boundary mapping we construct implies that dynamics in the bulk is dual to boundary dynamics with some of the qualitative features of AdS/CFT duality. In particular we show that the formation of a (toy model) black hole in the bulk dynamics is dual to a boundary dynamics in which local excitations unitarily evolve to a non-local excitation that lives outside the code space.

On the other hand, our construction shows that *any* local Hamiltonian in the bulk has a corresponding local boundary model. This implies that,

at least in these toy models, the holographic duality has less to do with (toy models of) quantum gravity per se, but is entirely a consequence of the hyperbolic geometry.

The main limitation of our result is the usual one stemming from the use of perturbation gadgets: the coupling strengths  $\alpha_{ij}$  in the boundary Hamiltonian  $H_{\text{bulk}}$  are very far from uniform. Indeed, some coupling strengths will be  $O(1)$  whilst others are  $O(\Delta_L)$ , where  $\Delta_L$  must be large to obtain a good simulation (at least  $\Delta_L = \Omega(\Lambda^{\text{poly}(n \log(n))})$ ) where  $\Lambda$  is the maximum strength of the local interactions in  $H_{\text{bulk}}$ .) High-energy interactions on the boundary perhaps matter less here than in Hamiltonian complexity results, since the motivation for holographic duality is to model high-energy physics phenomena. Nonetheless, it would be interesting to understand if a large range of interaction energy scales is a necessary feature of toy models of holographic duality, or an artefact of our proof techniques.

Our construction also inherits some of the drawbacks of the HaPPY code. In particular, the Ryu-Takayanagi formula is not obeyed exactly for arbitrary bulk regions; there exist certain pathological choices of boundary region,  $A$ , for which there are bulk operators that are not recoverable on  $A$  nor on  $A^c$  (violating complementary recovery). Like the HaPPY code, the tensor network cannot describe sub-AdS geometry as it is only defined at scales larger than the AdS radius. A number of holographic codes have been constructed which build on the HaPPY code and do not have these drawbacks. Notable examples include bidirectional holographic codes (BHC) composed of pluperfect tensors [43], and random tensor network constructions [21]. It would be interesting to apply the framework developed in this paper to stabilizer BHCs, and stabilizer random tensor networks [29] to construct a complete toy model of holographic duality which remedies these drawbacks.

## Acknowledgements

The authors would like to thank Eva Silverstein for very helpful discussions about holographic dualities, and Fernando Pastawski for explaining holographic tensor network constructions, during the 2017 KITP programme on Quantum Physics of Information. This research was supported in part by the National Science Foundation under Grant No. NSF PHY-1748958. TK is supported by the EPSRC Centre for Doctoral Training in Delivering Quantum Technologies [EP/L015242/1]. TC is supported by the Royal Society.

## References

- [1] P. Abramenko and K. Brown. *Buildings Theory and Applications*. Graduate Texts in Mathematics. Springer, 2008.

- [2] D. Aharonov and M. Ben-Or. Fault-tolerant quantum computation with constant error. In *Proceedings of the 29th Annual ACM Symposium on Theory of Computing*, page 176, 1997.
- [3] X. D. Ahmed Almheiri and D. Harlow. Bulk locality and quantum error correction in Ads/CFT. *Journal of High Energy Physics*, 2015.
- [4] E. M. Andreev. On convex polyhedra in lobachevskii spaces. *Math. USSR Sbornik*, 1970.
- [5] J. Beckenstein. Black holes and entropy. *Physical Review D*, 1973.
- [6] S. Bravyi and M. Hastings. On complexity of the quantum Ising model. *Communications in Mathematical Physics*, 2017.
- [7] R. Cleve, D. Gottesman, and H.-K. Lo. How to share a quantum secret. *Physical Review Letters*, 1999.
- [8] A. M. Cohen. Finite coxeter groups. <http://www.win.tue.nl/amc/buek/B13.ps>.
- [9] T. Cubitt, A. Montanaro, and S. Piddock. Universal Quantum Hamiltonians. *arxiv preprint arXiv:1701.05182*, 2017.
- [10] M. W. Davis. *The geometry and topology of Coxeter groups*. Princeton University Press, 2007.
- [11] A. Felikson and P. Tumarkin. Hyperbolic coxeter polytopes. <http://www.maths.dur.ac.uk/users/anna.felikson/Polytopes/polytopes.html>.
- [12] V. Gheorghiu. Standard form of qudit stabilizer groups. *Physics Letters A*, 2014.
- [13] D. Gottesman. *Stabilizer Codes and Quantum Error Correction*. PhD thesis, Caltech, 1997.
- [14] G. Gour and N. R. Wallach. All maximally entangled four-qubit states. *Journal of Mathematical Physics*, 2010.
- [15] D. Goyeneche, D. Alsina, J. I. Latorre, A. Riera, and K. Życzkowski. Absolutely maximally entangled states, combinatorial design and multi-unitary matrices. *Physical Review A*, 2015.
- [16] M. Grassl, T. Beth, and M. Roetteler. On optimal quantum codes. *International Journal of Quantum Information*, 2004.
- [17] M. Grassl and M. Roetteler. Quantum mds codes over small fields. In *IEEE International Symposium on Information Theory*, 2015.

- [18] R. Guglielmetti. CoxiterWeb. <https://coxiterweb.rafaelguglielmetti.ch>.
- [19] D. Harlow. The ryu-takayanagi formula from quantum error correction. *arXiv:1607.03901v2 [hep-th]*, 2016.
- [20] S. W. Hawking. Particle creation by black holes. *Communications in Mathematical Physics*, 1975.
- [21] P. Hayden et al. Holographic duality from random tensor networks. *JHEP*, 2016.
- [22] W. Helwig. Absolutely maximally entangled qudit graph states. *preprint arXiv:1306.2879*, 2013.
- [23] W. Helwig and W. Cui. Absolutely maximally entangled states: Existence and applications. *preprint arXiv:1306.2536*, 2013.
- [24] W. Helwig, W. Cui, A. Riera, J. I. Latorre, and H.-K. Lo. Absolute maximal entanglement and quantum secret sharing. *Physical Review A*, 2012.
- [25] F. Huber, O. Guene, and J. Siewert. Absolutely maximally entangled states of seven qubits do not exist. *Physical Review Letters*, 2017.
- [26] J. Kempe, A. Kitaev, and O. Regev. The complexity of the local Hamiltonian problem. *SIAM Journal of Computing*, 2006.
- [27] A. L. M. Headrick, V.E. Hubeny and M. Rangamani. Causality and holographic entanglement entropy. *Journal of High Energy Physics*, 2014.
- [28] J. M. Maldacena. Eternal black holes in anti-de Sitter. *JHEP*, 2003.
- [29] S. Nezami and M. Walter. Multipartite entanglement in stabilizer tensor networks. *arxiv preprint arxiv:1608.02595*, 2017.
- [30] R. Oliveira and B. Terhal. The complexity of quantum spin systems on a two-dimensional square lattice. *Quantum Information and Computation*, 8(10), 2005.
- [31] F. Pastawski, B. Yoshida, D. Harlow, and J. Preskill. Holographic quantum error-correcting codes: toy models for the bulk/boundary correspondence. *Journal of High Energy Physics*, 2015.
- [32] S. Piddock and A. Montanaro. The complexity of antiferromagnetic interactions and 2d lattices. *Quantum Information and Computation*, 2017.
- [33] E. M. Rains. Quantum codes of minimum distance two. *IEEE Transactions on Information Theory*, 1999.

- [34] I. Reed and G. Solomon. Polynomial codes over certain finite fields. *Journal of the Society for Industrial and Applied Mathematics*, 1960.
- [35] S. Ryu and T. Takayanagi. Aspects of holographic entanglement entropy. *Journal of High Energy Physics*, 2006.
- [36] S. Ryu and T. Takayanagi. Holographic derivation of entanglement entropy from AdS/CFT. *Physical Review Letters*, 2006.
- [37] G. Seroussi and R. Roth. On MDS extensions of generalized Reed-Solomon codes. *Information Theory, IEEE Transactions on*, 32, 1986.
- [38] B. Swingle. Constructing holographic spacetimes using entanglement renormalization. *arxiv preprint arXiv:1209.3304*, 2012.
- [39] B. Swingle. Entanglement renormalization and holography. *Physical Review D*, 2012.
- [40] J. Tits. Groupes et géométries de Coxeter. Unpublished manuscript, 1961.
- [41] E. B. Vinberg. Hyperbolic reflection groups. *Russian Math. Surveys*, 1985.
- [42] J. Weeks. Kaleidotile. <http://geometrygames.org/KaleidoTile/index.html>.
- [43] Z. Yang, P. Hayden, and X.-L. Qi. Bidirectional holographic codes and sub-ads locality. *Journal of High Energy Physics*, 2016.